

A bound preserving cut discontinuous Galerkin method for one dimensional hyperbolic conservation laws

Pei Fu*, Gunilla Kreiss†, Sara Zahedi‡

Abstract

In this paper we present a family of high order cut finite element methods with bound preserving properties for hyperbolic conservation laws in one space dimension. The methods are based on the discontinuous Galerkin framework and use a regular background mesh, where interior boundaries are allowed to cut through the mesh arbitrarily. Our methods include ghost penalty stabilization to handle small cut elements and a new reconstruction of the approximation on macro-elements, which are local patches consisting of cut and un-cut neighboring elements that are connected by stabilization. We show that the reconstructed solution retains conservation and optimal order of accuracy. Our lowest order scheme results in a piecewise constant solution that satisfies a maximum principle for scalar hyperbolic conservation laws. When the lowest order scheme is applied to the Euler equations, the scheme is positivity preserving in the sense that positivity of pressure and density are retained. For the high order schemes, suitable bound preserving limiters are applied to the reconstructed solution on macro-elements. In the scalar case, a maximum principle limiter is applied, which ensures that the limited approximation satisfies the maximum principle. Correspondingly, we use a positivity preserving limiter for the Euler equations, and show that our scheme is positivity preserving. In the presence of shocks additional limiting is needed to avoid oscillations, hence we apply a standard TVB limiter to the reconstructed solution. The time step restrictions are of the same order as for the corresponding discontinuous Galerkin methods on the background mesh. Numerical computations illustrate accuracy, bound preservation, and shock capturing capabilities of the proposed schemes.

Keywords: Hyperbolic conservation laws, discontinuous Galerkin method, cut elements, satisfying maximum principle, positivity preserving

1 Introduction

In this paper we consider problems in one space dimension, both scalar hyperbolic conservation laws and the important hyperbolic system of equations known as the Euler equations of gas dynamics. These are of the form

$$\begin{cases} \mathbf{u}_t + \partial_x \mathbf{f}(\mathbf{u}) = 0, & x \in \Omega, t > 0, \\ \mathbf{u}(x, 0) = \mathbf{u}_0(x), & x \in \Omega, \end{cases} \quad (1.1)$$

*School of Mathematics, Nanjing University of Aeronautics and Astronautics, 211106 Nanjing, China. E-mail: fu.pei@nuaa.edu.cn.

†Division of Scientific Computing, Department of Information Technology, Uppsala University, SE-75105 Uppsala, Sweden. E-mail: gunilla.kreiss@it.uu.se.

‡Department of Mathematics, KTH Royal Institute of Technology, SE-10044 Stockholm, Sweden. Email: sara.zahedi@math.kth.se.

with suitable boundary conditions. Here, $\Omega \subset \mathbb{R}$, $\mathbf{u} = (u_1, \dots, u_n)^T$ is a vector of real valued functions, which represents conservative variables, and $\mathbf{f}(\mathbf{u}) = (f_1(\mathbf{u}), \dots, f_n(\mathbf{u}))^T$ is the vector valued flux function. We assume that the corresponding Jacobian matrix has n real eigenvalues and n complete eigenvectors. Solutions of such systems may develop shocks or discontinuities even if the initial data is smooth. It therefore becomes necessary to consider weak solutions, and as usual we seek the physical relevant weak solution which satisfies an entropy condition.

An important property of the entropy solution for a scalar equation of the form (1.1) is the maximum principle, which for Cauchy problems means

$$\text{if } \mathbf{u}_0(x) \in [\mathbf{m}, \mathbf{M}] \text{ then } \mathbf{u}(x, t) \in [\mathbf{m}, \mathbf{M}]. \quad (1.2)$$

The solution of the Euler equations usually does not satisfy the maximum principle, but density and pressure should remain positive. With negative density or pressure hyperbolicity is lost and the Euler system becomes ill-posed, which causes severe numerical difficulties. For initial boundary-value problems boundary conditions must satisfy corresponding restraints for the maximum principle, or positivity, to be valid. It has been noted that high order methods without bound preserving properties often suffer from numerical instability or nonphysical features when applied to problems with low density or high Mach number, see for example [25].

A finite element method (FEM) based on discontinuous piecewise polynomial spaces is commonly called a discontinuous Galerkin (DG) method. The DG methodology coupled to explicit Runge-Kutta time discretizations and limiters, has successfully been applied to nonlinear time dependent hyperbolic conservation laws, see e.g. [13, 12, 14]. For more details on DG methods, we refer to [28, 44]. Most finite element methods require the mesh to be aligned to boundaries and material interfaces, and to achieve the optimal accuracy the mesh quality needs to be high.

For boundaries and material interfaces with complicated shapes one approach is to start with a Cartesian background mesh and use agglomeration to create a body fitted mesh of good quality. An alternative approach is to allow boundaries and interfaces to cut through the Cartesian background mesh arbitrarily. This is the approach we take. In this paper we develop an unfitted discretization for hyperbolic PDEs based on standard Cartesian finite elements that preserves important properties. Small cut elements may cause problems, including ill-conditioned linear systems and severe time-step restrictions. Various techniques have been introduced to handle such difficulties. One approach often used in unfitted methods based on DG is cell merging, where new elements, still unfitted but of sufficient size are created by merging small cut elements with their neighbours [30, 32, 38, 39, 40, 9, 10]. A common technique in connection with Cut Finite Element Methods (CutFEM) is to add ghost penalty stabilization terms in the weak form [4, 5, 36, 42, 24]. In CutFEM the physical domain is embedded into a computational domain equipped with a quasi-uniform mesh. Elements that have an intersection with the domain of interest define the active mesh and associated to that is a finite dimensional function space and a weak form, which together define the numerical scheme [35, 26, 17, 46]. Interface and boundary conditions are imposed weakly, when the mesh is unfitted.

Recently, some methods based on the DG framework with time-step restrictions that are independent of the sizes of smallest elements have been developed for time-dependent hyperbolic conservation laws. In [16, 37] methods are presented that include stabilization of small elements, designed to restore proper domains of dependence. In [21] small elements are stabilized by a redistribution step, which was first introduced in [3]. In [19] a family of high-order cut discontinuous Galerkin (Cut-DG) methods with ghost penalty stabilization for non-linear scalar hyperbolic problems is presented. These methods are proven to be high order accurate and L^2 -stable under time-step restrictions that are independent of cut sizes. Total variation stability, which is important when considering problems with shocks, is also established, but only for the piecewise constant

scheme. In [18] a similar methodology is used, but the focus is on conservation at material interfaces with discontinuous fluxes, which cut arbitrarily through elements in one and two space dimensions.

In this paper we will develop and analyze a family of high order bound-preserving unfitted discontinuous Galerkin (DG) methods for nonlinear hyperbolic conservation laws. We will consider (1.1) with several artificial subdomain interfaces, a problem which is equivalent to (1.1) on the original domain. The computational mesh, which will be introduced later, is not fitted to these interfaces. We have chosen this model problem as a one dimensional model for problems in higher spatial dimension with a physical boundary or a physical interface that cuts arbitrarily through the computational mesh and creates increasingly many cut elements as the mesh is refined, see Figure 1.

The contribution in this paper is a method for applying limiters in connection with unfitted discretizations such as in [19] so that bound preservation is achieved for piecewise constant schemes as well as for high order schemes. We illustrate with numerical experiments (see Figure 4, 6 in Section 5) that it is not sufficient to directly apply limiters on the numerical solution on the unfitted computational mesh. We show that the desired properties can be achieved on macro-elements. Macro-elements [33] consist of cut and un-cut neighbouring elements in the computational mesh so that each macro-element always has a large intersection with the domain of interest. We propose a reconstruction of the approximated solution on macro-elements based on polynomial extension that preserves conservation and order of accuracy. If reconstruction is applied everywhere the proposed scheme corresponds to cell merging with a particular basis on the macro-element. To minimize errors the reconstruction on a macro-element should be applied only when limiting is needed on an element belonging to the macro-element. This is possible when the ill-conditioning and time step restrictions due to small cut cells is handled by ghost penalty terms.

In the piecewise constant case we can show that under a suitable time step restriction the reconstructed solutions in the scalar case and for the Euler system, satisfy the maximum principle and the positivity of density and pressure, respectively. For the higher order schemes we can show that the average values of the reconstructed solutions on the macro-elements satisfy the corresponding bounds. Thus, the bound preserving limiters developed by Zhang et. al [52, 53] can be applied to ensure that the discrete approximations satisfy the pointwise bounds.

The bound preserving limiter is not enough to control oscillations near shocks. There we need additional limiting. In our work, we use a TVD/TVB slope limiter commonly applied in combination with DG methods, see [13, 12, 11, 14]. Other limiters, such as WENO-limiters [41] are also possible.

The paper is organized as follows. In Section 2 we introduce the model problem, the mesh, the finite element function spaces, the Cut-DG discretization, the process for reconstructing solutions on macro-elements, and some notation. In Section 3 the scheme is presented for scalar hyperbolic conservation laws and we show that it satisfies the maximum-principle property when a suitable bound preserving limiter is applied during time evolution. In Section 4, we present the corresponding scheme for the Euler equations, and analyze the positivity property. In Section 5 numerical computations are presented, which support the theoretical results. Finally, a conclusion is given in Section 6.

2 A cut discontinuous Galerkin discretization in space

In this section we present an unfitted spatial discretization for hyperbolic conservation laws on the form (1.1). After presenting the model problem we define the mesh, our finite dimensional function spaces, and the macro-element partition.

2.1 A model geometry in one space dimension

To mimic a problem in higher spatial dimensions with a boundary (or an interface) that cuts arbitrarily through a computational mesh, as in Figure 1, we consider a one dimensional problem with several artificial interfaces, see Figure 2. In the computations in Section 5 we let the number of cut elements increase with mesh refinement. This one dimensional problem is considerably more challenging than if only cut elements at the two boundaries are present. For completeness, results with unfitted boundaries and with a physical interface are included in subsections 5.4.4 and 5.3.

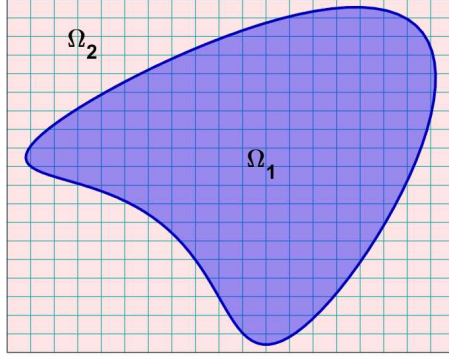


Figure 1: An illustration of a regular mesh and an unfitted interface.

2.2 Mesh and spaces

We embed the physical domain $\Omega = [x_L, x_R]$ into a computational domain $\Omega_h = [x_L, x_R]$, which is discretized into N intervals $I_j = [x_{j-\frac{1}{2}}, x_{j+\frac{1}{2}}]$, $j = 1, \dots, N$ such that $x_L = x_{\frac{1}{2}} < x_{\frac{3}{2}} < \dots < x_{N+\frac{1}{2}} = x_R$, where $x_{j+\frac{1}{2}} = x_L + jh$ with $h = \frac{x_R - x_L}{N}$. Let

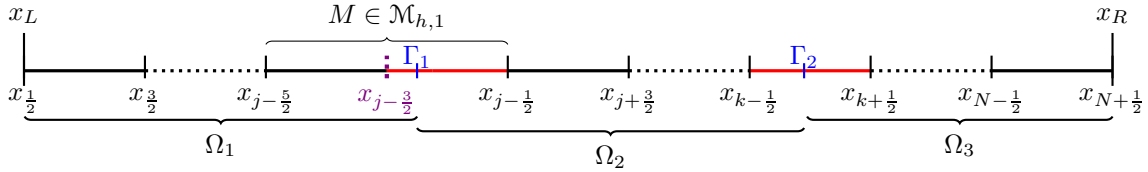


Figure 2: Discretization of the computational domain $\Omega_h = [x_L, x_R]$ into a uniform partition. This background mesh is cut by two interfaces at $x = \Gamma_1$ and $x = \Gamma_2$, dividing the computational domain into three subdomains. The dotted line at $x_{j-\frac{3}{2}}$ indicates the interior edge in $\mathcal{M}_{h,1}$ on which stabilization is applied, i.e. $x_{j-\frac{3}{2}} \in \mathcal{F}_{h,1}$

$$\mathcal{T}_h = \{I_j : I_j \cap \Omega \neq \emptyset : j = 1, \dots, N\}. \quad (2.1)$$

We refer to \mathcal{T}_h as the background mesh of the domain Ω . The background mesh may be cut by either the outer domain boundary $\partial\Omega$ and by interior boundaries (interfaces). In this work we let

$$\Omega_h = \Omega = \bigcup_{j=1}^N I_j, \quad (2.2)$$

and hence the generated background mesh \mathcal{T}_h aligns with the boundary $\partial\Omega$ but not with interior interfaces. Assume the interior interfaces divide the domain into N_Ω non-overlapping subdomains Ω_i such that $\Omega = \cup_{i=1}^{N_\Omega} \Omega_i$. The $N_\Omega - 1$ interfaces are positioned at $x = \Gamma_j$, $j = 1, \dots, N_\Omega - 1$ and non of them align with the mesh, so we have $N_\Omega - 1$ cut elements in the interior of the domain Ω . For an illustration, see Figure 2.

Associated with the subdomains Ω_i we define active meshes

$$\mathcal{T}_{h,i} = \{I_j \in \mathcal{T}_h : I_j \cap \Omega_i \neq \emptyset\}, \quad i = 1, \dots, N_\Omega, \quad (2.3)$$

and active finite element spaces

$$V_{h,i}^p = \{v \in L^2(\Omega) : v|_{I_j} \in \mathbb{P}^p(I_j), \forall I_j \in \mathcal{T}_{h,i}\}, \quad (2.4)$$

where $\mathbb{P}^p(I_j)$ denotes the space of discontinuous piecewise polynomials of degree less or equal to p on I_j .

Let $\mathcal{E}_{h,i}$ be the set of interior edges in the active mesh $\mathcal{T}_{h,i}$. The intersections of I_j with Ω_i are in the set $\mathcal{K}_{h,i}$

$$\mathcal{K}_{h,i} = \{K = I_j \cap \Omega_i : I_j \in \mathcal{T}_{h,i}\}. \quad (2.5)$$

Finally, let

$$V_h^p = \bigoplus_{i=1}^{N_\Omega-1} V_{h,i}^p. \quad (2.6)$$

2.2.1 Macro-elements

We create a macro-element partition $\mathcal{M}_{h,i}$ of the active domain

$$\Omega_{h,i} = \bigcup_{I_j \in \mathcal{T}_{h,i}} I_j \quad (2.7)$$

following [33]. The idea is to construct elements with large Ω_i -intersections. To do that each interval I_j in the active mesh $\mathcal{T}_{h,i}$ is first classified as having a large or a small intersection with the domain Ω_i . We classify $I_j \in \mathcal{T}_{h,i}$ as having a large Ω_i -intersection if

$$\delta \leq \frac{|I_j \cap \Omega_i|}{|I_j|}. \quad (2.8)$$

Here $0 < \delta \leq 1$ is a constant which is independent of the element and of the mesh size h . We assume that h is small enough so that in each subdomain Ω_i there is at least one element which is classified as having a large intersection with Ω_i . To each element with a large intersection a macro-element is associated. The macro-element consist of either only this element or this element and adjacent elements (connected via a bounded number of internal edges) that are classified as having small intersections with Ω_i . In one space dimension a macro-element will at most consist of three elements. In higher dimensions, if the geometry is smooth and well resolved the macro-element partitioning can be made to avoid macro-elements of very different size, please see Algorithm 1 in [33].

We define by $\mathcal{F}_{h,i}(M)$ the set consisting of interior edges of macro-element $M \in \mathcal{M}_{h,i}$. Stabilization will be applied at these edges. Note that the set $\mathcal{F}_{h,i}(M)$ is empty when the macro-element consist of

only one element I_j (with a large Ω_i -intersection). An example is shown in Figure 2, where $M \in \mathcal{M}_{h,1}$ is a macro-element consisting of more than one element in $\Omega_{h,1}$ and $x_{j-\frac{3}{2}} \in \mathcal{F}_{h,1}$ is the interior edge of that macro-element. In the original ghost-penalty approach, stabilization is applied on all interior edges (with respect to Ω_i) that also belong to cut elements. This is referred to as full stabilization. Using the macro-element partitioning stabilization is applied only on interior edges in each macro-element and never between macro-elements, hence conservation properties of the underlying DG-scheme can be inherited to macro-elements. In addition, with a macro-element stabilization errors are less sensitive to stabilization parameters, see [33]. With smaller choices of δ less elements are connected via the stabilization, resulting in a more sparse mass-matrix. However a small value causes a more severe time step restriction, see e.g. Theorem 3.1. In the numerical experiments we have used $\delta = 0.2$.

2.3 The weak formulation

As a first step in finding an approximate solution to (1.1), we follow [19, 18] and formulate a semi-discrete weak form: For $t \in [0, T]$ find $\mathbf{u}_h(\cdot, t) = (\mathbf{u}_{h,1}(\cdot, t), \dots, \mathbf{u}_{h,N_\Omega}(\cdot, t)) \in V_h^p$ such that,

$$((\mathbf{u}_h)_t, \mathbf{v}_h)_\Omega + \gamma_1 J_1(\mathbf{u}_{h,t}, \mathbf{v}_h) + a(\mathbf{u}_h, \mathbf{v}_h) + \gamma_0 J_0(\mathbf{u}_h, \mathbf{v}_h) = 0, \quad \forall \mathbf{v}_h \in V_h^p, \quad (2.9)$$

where

$$(\mathbf{u}_t, \mathbf{v})_\Omega = \sum_{i=1}^{N_\Omega} \sum_{K \in \mathcal{K}_{h,i}} ((\mathbf{u}_i)_t, \mathbf{v}_i)_K, \quad (2.10)$$

$$a(\mathbf{u}, \mathbf{v}) = - \sum_{i=1}^{N_\Omega} \sum_{K \in \mathcal{K}_{h,i}} (\mathbf{f}(\mathbf{u}_i), \partial_x(\mathbf{v}_i))_K - \sum_{i=1}^{N_\Omega} \sum_{e \in \mathcal{E}_{h,i}} \widehat{\mathbf{f}}(\mathbf{u}_i)_e [\mathbf{v}_i]_e - \sum_{i=1}^{N_\Omega-1} \widehat{\mathbf{f}}(\mathbf{u})_{\Gamma_i} [\mathbf{v}]_{\Gamma_i}, \quad (2.11)$$

$$J_s(\mathbf{u}, \mathbf{v}) = \sum_{i=1}^{N_\Omega} \sum_{M \in \mathcal{M}_{h,i}} \sum_{e \in \mathcal{F}_{h,i}(M)} \sum_{k=0}^p \omega_k h^{2k+s} [\partial^k \mathbf{u}_i]_e [\partial^k \mathbf{v}_i]_e. \quad (2.12)$$

Here

$$\widehat{\mathbf{f}}(\mathbf{u})_\xi = \{\mathbf{f}(\mathbf{u})\}_\xi - \frac{\lambda}{2} [\mathbf{u}]_\xi \quad (2.13)$$

is the Lax-Friedrichs flux, where λ is an estimate of the largest absolute eigenvalue of the Jacobian matrix $\frac{\partial \mathbf{f}}{\partial \mathbf{u}}$ in the domain Ω , $[\mathbf{w}]_\xi = \mathbf{w}^+ - \mathbf{w}^-$ represents the jump of the function \mathbf{w} at ξ and $\{\mathbf{w}\}_\xi = \frac{(\mathbf{w}^+ + \mathbf{w}^-)}{2}$ with $\mathbf{w}^+ = \lim_{\epsilon \rightarrow 0^+} \mathbf{w}(\xi + \epsilon)$, and $\mathbf{w}^- = \lim_{\epsilon \rightarrow 0^+} \mathbf{w}(\xi - \epsilon)$ denoting the limit values of $\mathbf{w} \in V_h^p$ at ξ from right and left. Note that at $e \in \mathcal{E}_{h,i}$ we have $[\mathbf{v}]_e = \mathbf{v}_i^+ - \mathbf{v}_i^-$ and at Γ_i we have $[\mathbf{v}]_{\Gamma_i} = \mathbf{v}_{i+1}|_{\Gamma_i} - \mathbf{v}_i|_{\Gamma_i}$ with $\mathbf{v}_i \in V_{h,i}^p$. In this paper we apply the global Lax-Friedrichs flux, i.e. λ is constant in the entire domain Ω . The local Lax-Friedrichs flux [27] and other positivity preserving fluxes like HLL flux [49], HLLC flux [2] can also be applied.

In the stabilization term (2.12), $\omega_k = \frac{1}{(k!)^2(2k+1)}$, we refer to [47] for more details about this choice. The stabilization parameters γ_0, γ_1 are positive constants and need to be chosen sufficiently large to avoid severe time step restrictions. In our numerical experiments $\gamma_0 = 0.25$ and $\gamma_1 = 0.75$. Assuming time and space scaled so that the wave speed is $\mathcal{O}(1)$ these values work well. However, we have not optimized these values but with the macro-element stabilization our experience is that the results are not sensitive to these precise values.

The initial condition is given by the stabilized L^2 -projection:

$$\sum_{i=1}^{N_\Omega} \sum_{K \in \mathcal{K}_{h,i}} (\mathbf{u}_h(\cdot, 0), \mathbf{v}_h)_K + \gamma_1 J_1(\mathbf{u}_h(\cdot, 0), \mathbf{v}_h) = \sum_{i=1}^{N_\Omega} \sum_{K \in \mathcal{K}_{h,i}} (\mathbf{u}_0, \mathbf{v}_h)_K, \quad \forall \mathbf{v}_h \in V_h^p. \quad (2.14)$$

2.4 A reconstruction on macro-elements

In general, fully discrete solutions of (2.9) do not automatically satisfy the maximum principle for scalar equations (see the left panel in Figure 5), or positivity of density and pressure for the Euler equations. To guarantee that the approximate solution to (1.1) has all the desired properties we utilize limiters, but we need to apply them properly. We will need a bound preserving limiter and sometimes when shocks or discontinuities are present we will also need additional limiters. The numerical examples in Section 5 show that it does not suffice to apply a standard limiter directly. Our main idea is to define an approximate solution $\mathbf{u}_{h,M}$ from \mathbf{u}_h on the macro-element partition of the subdomains, and apply the appropriate limiters on $\mathbf{u}_{h,M}$.

We will in next sections show that applying a limiter to the reconstructed solution on macro elements will ensure the bound preserving properties.

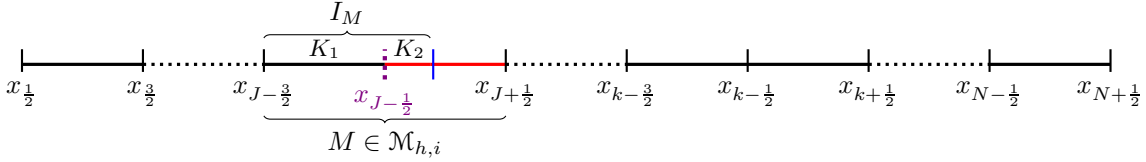


Figure 3: Illustration of intervals $K_j \in \mathcal{K}_{h,i}$, which constitute part of the macro-element M .

For each macro-element $M \in \mathcal{M}_{h,i}$, see Figure 3, let

$$I_M = M \cap \Omega_i = \cup_{j \in N_M} K_j \text{ with } K_j \in \mathcal{K}_{h,i}, \quad (2.15)$$

where N_M is an index set for those elements in $\mathcal{K}_{h,i}$ that constitute I_M , the part of the macro-element M that is in Ω_i . Furthermore, we have $|I_M| \geq \delta h$ with the definition of δ in (2.8). For the macro-element M illustrated in Figure 3, $N_M = 1, 2$. We consider the scalar function on the macro-element here and note that we do a reconstruction for each component of \mathbf{u}_h if \mathbf{u}_h is a vector-valued function. Let $u_h(\cdot, t) = (u_{h,1}, \dots, u_{h,N_\Omega})$ with $u_{h,i} \in V_{h,i}^p$ be an approximation of $u(\cdot, t)$. and let $u_i = u|_{\Omega_i}$.

For each macro-element $M \in \mathcal{M}_{h,i}$ and each K_j with $j \in N_M$ define

$$w_{h,j} = u_{h,i}|_{K_j}, \quad w_{h,j}^e = E_M w_{h,j}, \quad (2.16)$$

where E_M is the polynomial extension operator that extends $w_{h,j}$ to the entire macro-element M , such that

$$E_M w_{h,j}|_{K_j} = w_{h,j}, \quad \|E_M w_{h,j}\|_{I_M} \leq c \|w_{h,j}\|_{K_j}. \quad (2.17)$$

Here $c = \tilde{c} \frac{\sqrt{|I_M|}}{\sqrt{|K_j|}}$ and \tilde{c} is a constant independent of mesh size h and independent of how the interface cuts through the element. At a point x outside K_j , $w_{h,j}^e(x)$ is simply the evaluation of the polynomial at x .

We propose the following reconstruction on each M

$$u_{h,i}^M = \sum_{j \in N_M} \omega_j w_{h,j}^e + c_0, \quad \text{for each } M \in \mathcal{M}_{h,i} \quad (2.18)$$

with

$$\omega_j = \frac{|K_j|}{|I_M|}, \quad c_0 = \frac{\sum_{j \in N_M} \int_{K_j} w_{h,j} dx}{|I_M|} - \frac{\sum_{j \in N_M} \omega_j \int_{I_M} w_{h,j}^e dx}{|I_M|}. \quad (2.19)$$

Note that each $w_{h,j}$ is extended to the entire macro-element and evaluated in I_M and other choices of weights are possible. The constant c_0 is chosen so that $u_{h,i}^M$ has the same mean value on I_M as $u_{h,i}$. Note that $\sum_{j \in N_M} \omega_j = 1$, and when M consists of only one element then $|K_j| = |I_M|$ and $u_{h,i}^M = u_{h,i}|_M$.

This reconstruction yields a new approximate solution $u_{h,i}^{\mathcal{M}}$ on the macro-element partition, which is in the subspace of $V_{h,i}^p$ and has the following properties

- conservation: we have

$$\int_{I_M} u_{h,i}^{\mathcal{M}} dx = \sum_{j \in N_M} \int_{K_j} w_{h,j} dx = \int_{I_M} u_{h,i} dx, \quad (2.20)$$

which shows that the reconstruction maintains conservation.

- accuracy: to consider the error estimate of the reconstruction, we write

$$\begin{aligned} \|u_i - u_{h,i}^{\mathcal{M}}\|_{I_M} &= \left\| \sum_{j \in N_M} \omega_j (u_i - w_{h,j}^e) - c_0 \right\|_{I_M} = \left\| \sum_{j \in N_M} \omega_j (u_i - w_{h,j}^e) \right. \\ &\quad \left. + \sum_{j \in N_M} \frac{1}{|I_M|} \int_{K_j} (u_i - w_{h,j}) dx + \sum_{j \in N_M} \frac{\omega_j}{|I_M|} \int_{I_M} (w_{h,j}^e - u_i) dx \right\|_{I_M} \\ &\leq \left\| \sum_{j \in N_M} \omega_j (u_i - w_{h,j}^e) \right\|_{I_M} + \left\| \sum_{j \in N_M} \frac{\omega_j}{|I_M|} \int_{I_M} (w_{h,j}^e - u_i) dx \right\|_{I_M} + \frac{1}{|I_M|} \left\| \sum_{j \in N_M} \int_{K_j} (u_i - w_{h,j}) dx \right\|_{I_M} \\ &\leq \sum_{j \in N_M} \omega_j \|u_i - w_{h,j}^e\|_{I_M} + \sum_{j \in N_M} \frac{\omega_j}{|I_M|} \sqrt{|I_M|} \int_{I_M} |w_{h,j}^e - u_i| dx + \sum_{j \in N_M} \frac{1}{\sqrt{|I_M|}} \int_{K_j} |u_i - w_{h,j}| dx \\ &\leq 2 \sum_{j \in N_M} \omega_j \|u_i - w_{h,j}^e\|_{I_M} + \sum_{j \in N_M} \sqrt{\omega_j} \|u_i - w_{h,j}\|_{K_j} \\ &\leq (2\tilde{c} + 1) \sum_{j \in N_M} \sqrt{\omega_j} \|\pi_h u_i - w_{h,j}\|_{K_j} + 3 \sum_{j \in N_M} \sqrt{\omega_j} \|u_i - \pi_h u_i\|_{I_M}. \end{aligned} \quad (2.21)$$

Here $\pi_h : u_i \in H^{p+1}(\Omega_i) \rightarrow \pi_h(Eu_i|_{\mathcal{M}_{h,i}}) \in V_{h,i}^p$ is the projection operator where E is a Sobolev extension operator [45]. Note that we have used $\sum_{j \in N_M} \omega_j = 1$, and added and subtracted $\frac{1}{|I_M|} \int_{I_M} u_i dx = \frac{1}{|I_M|} \sum_{j \in N_M} \int_{K_j} u_i dx = \frac{1}{|I_M|} \sum_{j \in N_M} \omega_j \int_{I_M} u_i dx$ in the second equality in (2.21). To get the inequalities in the third and fourth line we used Minkowski's inequality. In the fifth line, Hölder's inequality is applied. To get the last inequality in (2.21), we split $u_i - w_{h,j}^e$ into two terms $u_i - \pi_h u_i$ and $\pi_h u_i - w_{h,j}^e$. We note that $u_i = u|_{\Omega_i}$ and we have $\pi_h u_i = \pi_h(Eu_i|_{\mathcal{M}_{h,i}})$. Thus $\pi_h u_i - w_{h,j}^e$ is a polynomial extension of $\pi_h u_i - w_{h,j}$ from element K_j to the entire macro-element M . From (2.17), we have $\omega_j \|\pi_h u_i - w_{h,j}^e\|_{I_M} \leq \tilde{c} \sqrt{\omega_j} \|\pi_h u_i - w_{h,j}\|_{K_j}$. With optimal error estimates for the projection operator, it follows that the reconstructed solution has the same order of accuracy as the original u_h . We refer to [18] for the estimate of $\sum_{j \in N_M} \|\pi_h u_i - w_{h,j}\|_{K_j}$. Thus, the reconstruction does not destroy the order of accuracy of the numerical solution.

Remark 2.1. In practice the approximate solution $\mathbf{u}_{h,M}$ should be constructed only when limiting is necessary. Numerical experiments, where the reconstruction is only done for macro-elements that violate the bound property, show that this works well. See Figure 7 for a scalar example and Figure 13 for a system. We remark that it is also possible to use the extension technique in the discretization of the PDE instead of adding stabilization terms, see for example [29, 7, 6].

3 Maximum principle preserving DG methods for scalar equations

In this section, we propose a fully discretized scheme for the scalar hyperbolic conservation laws and study the maximum principle property of the proposed scheme. It suffices to consider the forward Euler method. In the numerical experiments, we use high order time discretization methods that are linear combinations of the forward Euler method. In each time step we include a reconstruction on the macro-element partition of the mesh. We will show that our proposed scheme satisfies the maximum principle. The scheme can be summarized as follows: Given the approximate solution $u_h^n = (u_{h,1}^n, \dots, u_{h,N_\Omega}^n)$ with $u_{h,i}^n \in V_{h,i}^p$, and satisfying $u_{h,i}^n|_{\Omega_i} \in [\mathfrak{m}, \mathfrak{M}]$ at time t_n , we compute u_h^{n+1} by the following steps:

1. Find $\tilde{u}_h^{n+1} = (\tilde{u}_{h,1}^{n+1}, \tilde{u}_{h,2}^{n+1}, \dots, \tilde{u}_{h,N_\Omega}^{n+1}) \in V_h^p$ such that for $\forall v_h \in V_h^p$

$$\sum_{i=1}^{N_\Omega} \sum_{K \in \mathcal{K}_{h,i}} \left(\frac{\tilde{u}_{h,i}^{n+1} - u_h^n}{\Delta t}, v_h \right)_K + \gamma_1 J_1 \left(\frac{\tilde{u}_h^{n+1} - u_h^n}{\Delta t}, v_h \right) + a(u_h^n, v_h) + \gamma_0 J_0(u_h^n, v_h) = 0, \quad (3.1)$$

with the bilinear forms $a(\cdot, \cdot)$ and $J_s(\cdot, \cdot)$ ($s = 0, 1$) defined as in (2.11) and (2.12).

2. From $\tilde{u}_{h,i}^{n+1}$, we compute the reconstructed solution following (2.18). For each $M \in \mathcal{M}_{h,i}, i = 1, \dots, N_\Omega$, we compute $u_{h,i}^{\mathcal{M},n+1}$ from $\tilde{u}_{h,i}^{n+1}$, which is

$$u_{h,i}^{\mathcal{M},n+1}|_M = \frac{\sum_{j \in N_M} |K_j| \tilde{w}_{h,j}^{e,n+1}}{|I_M|} + c_0. \quad (3.2)$$

Here, $\tilde{w}_{h,j}^{e,n+1}$ is defined as in (2.16) but $u_{h,i}$ is replaced by $\tilde{u}_{h,i}^{n+1}$. If needed, bound preserving limiting, which will be described in section 3.3, is applied to the reconstructed solution before the next step.

3. Finally, for each macro-element $M \in \mathcal{M}_{h,i}, i = 1, \dots, N_\Omega$ set

$$u_{h,i}^{n+1}|_M = u_{h,i}^{\mathcal{M},n+1}|_M. \quad (3.3)$$

At the initial time t_0 , given u_0 , replace (3.1) by (2.14) and then apply step 2 and 3 to compute $u_{h,i}^{M,0}$ and $u_{h,i}^0$. In practice, the approximate solution $\mathbf{u}_{h,M}$ should be construct only in those $M \in \mathcal{M}_{h,i}$ when limiting is needed (see Figure 7 for Burgers' equation and Figure 13 for the Euler equations). Note that the stabilization terms J_i act only on the interior edges in macro-elements. For macro-elements where the reconstruction is done, the reconstructed solution u_h^n has no jump across the interior edges and thus on such elements the stabilization terms $J_i(u_h^n, v_h)$ vanish. In all other macro-elements the stabilization J_0 is needed.

In the higher order versions of our scheme the reconstructed solution may not satisfy the maximum principle automatically at the next time level i.e. $u_{h,i}^{\mathcal{M},n+1} \notin [\mathfrak{m}, \mathfrak{M}], i = 1, \dots, N_\Omega$, and this makes limiting necessary. The details are found in Algorithm 1.

3.1 Piecewise constant approximation

Let $u_h^n \in V_h^p, p = 0$ denote the piecewise constant function that approximates the solution at time t_n . Note that in this case, we have from the conservation property (2.18) that $c_0 = 0$ and thus

$$su_{h,i}^{M,n} = \frac{\sum_{j \in N_M} |K_j| \tilde{w}_{h,j}^n}{|I_M|}, \quad (3.4)$$

where $\tilde{w}_{h,j}^n$ denotes the mean value on the element K_j . Note that the solution $u_{h,i}^{\mathcal{M},n}$ has no discontinuity at interior edges of macro-elements (for example across the edge between K_1 and K_2 in Figure 3), and with $p = 0$ there is no difference between function values and mean values.

Theorem 3.1. Consider the Cut-DG scheme described by (3.1)-(3.3) with $p = 0$. If the time step Δt satisfies

$$\frac{\Delta t}{\delta h} \lambda \leq 1, \quad (3.5)$$

then $u_{h,i}^n|_{\Omega_i} \in [\mathbf{m}, \mathbf{M}]$, $i = 1, \dots, N_\Omega$ implies $u_{h,i}^{n+1}|_{\Omega_i} \in [\mathbf{m}, \mathbf{M}]$ for $i = 1, \dots, N_\Omega$. Here h is the element size in the background mesh, and δ is a given constant, which in (2.8) defines when an intersection between an element and Ω_i is classified as large. λ is the maximum absolute value of the Jacobian $\partial f(u_h^n)/\partial u_h^n$ in the domain Ω .

Proof. By the reconstruction (3.3), u_h^n is constant in each macro element $M \in \mathcal{M}_{h,i}$, $i = 1, \dots, N_\Omega$, and we denote the value by $u_{h,i}^{M,n}$. Let $u_{h,l}^n$ and $u_{h,r}^n$ denote the values adjacent to the left and right boundary of I_M , respectively, see I_M in (2.15). We assume $u_h^n \in [m, M]$. Thus, we have $u_{h,i}^{M,n}, u_{h,l}^n, u_{h,r}^n \in [\mathbf{m}, \mathbf{M}]$. Further, let \widehat{f}_l and \widehat{f}_r denote the numerical fluxes on the left and on the right boundary of the macro-element I_M , respectively. We use the global Lax-Friedrichs flux, defined by (2.13), which is

$$\widehat{\mathbf{f}}_l = \frac{1}{2} \left(\mathbf{f}(u_{h,l}^n(x_l)) + \mathbf{f}(u_{h,i}^{M,n}(x_l)) \right) - \frac{\lambda}{2} \left(u_{h,i}^{M,n}(x_l) - u_{h,l}^n(x_l) \right), \quad (3.6)$$

$$\widehat{\mathbf{f}}_r = \frac{1}{2} \left(\mathbf{f}(u_{h,i}^{M,n}(x_r)) + \mathbf{f}(u_{h,r}^n(x_r)) \right) - \frac{\lambda}{2} \left(u_{h,i}^{M,n}(x_r) - u_{h,r}^n(x_r) \right). \quad (3.7)$$

Let the test function v_h in (3.1) to be $v_h = 1$ on each element of M and $v_h = 0$ otherwise. By noting that the stabilization terms J_s act only on interior edges in macro-elements and that $u_{h,i}^n$ has no jump across such edges, we get

$$\sum_{j \in N_M} |K_j| \widetilde{w}_{h,j}^{n+1} = \sum_{j \in N_M} |K_j| u_{h,i}^n|_{K_j} - \Delta t (\widehat{f}_r - \widehat{f}_l).$$

Taking (??) into account at $t = t_{n+1}$, the above equation can be written as

$$u_{h,i}^{M,n+1} = u_{h,i}^{M,n} - \frac{\Delta t}{|I_M|} (\widehat{f}_r - \widehat{f}_l). \quad (3.8)$$

With the definition of global Lax-Friedrichs flux (3.6)-(3.7) we can rewrite (3.8) as

$$u_{h,i}^{M,n+1} = u_{h,i}^{M,n} - \frac{\lambda \Delta t}{|I_M|} u_{h,i}^{M,n} + \frac{\Delta t}{2|I_M|} (\lambda u_{h,r}^n - f(u_{h,r}^n)) + \frac{\Delta t}{2|I_M|} (\lambda u_{h,l}^n + f(u_{h,l}^n)). \quad (3.9)$$

With $H(a, b, c)$ defined as

$$H(a, b, c; \lambda) := \left(1 - \frac{\lambda \Delta t}{|I_M|} \right) b + \frac{\Delta t}{2|I_M|} (\lambda c - f(c)) + \frac{\Delta t}{2|I_M|} (\lambda a + f(a)), \quad (3.10)$$

we have

$$u_{h,i}^{M,n+1} = H(u_{h,l}^n, u_{h,i}^{M,n}, u_{h,r}^n; \lambda). \quad (3.11)$$

Since $|I_M| \geq \delta h$, it follows by (3.5) that

$$0 < \frac{\Delta t}{|I_M|} \lambda \leq 1, \quad (3.12)$$

$$\frac{\partial H(a, b, c; \lambda)}{\partial a} = \frac{\Delta t}{2|I_M|} (\lambda + f'(a)) \geq 0, \quad (3.13)$$

$$\frac{\partial H(a, b, c; \lambda)}{\partial b} = 1 - \frac{\Delta t}{|I_M|} \lambda \geq 0, \quad (3.14)$$

$$\frac{\partial H(a, b, c; \lambda)}{\partial c} = \frac{\Delta t}{2|I_M|}(\lambda - f'(c)) \geq 0. \quad (3.15)$$

Further,

$$H(z, z, z; \lambda) = \left(1 - \frac{\lambda \Delta t}{|I_M|}\right) z + \frac{\Delta t}{2|I_M|}(\lambda z - f(z)) + \frac{\Delta t}{2|I_M|}(\lambda z + f(z)) = z. \quad (3.16)$$

Thus, it follows that $u_{h,i}^{M,n+1} \in [\mathfrak{m}, \mathfrak{M}]$ and hence u_h^{n+1} satisfies the maximum principle under the time step restriction (3.5). \square

3.2 Mean values of high order approximations

We now consider higher order schemes in space and time, where the time discretization can be seen as a sequence of Euler steps. We therefore consider (3.1) with $p \geq 1$ together with the reconstruction (3.2). We will show that for sufficiently small time steps the mean values on macro-elements after an Euler step satisfy the same maximum principle as in Theorem 3.1 above. We will follow the ideas used to prove the corresponding result for the standard DG method [52]. In the proof we will use the q -point Gauss-Lobatto quadrature rule on each macro-element, which is exact for polynomials of degree $2q - 3$. Let q be the smallest integer satisfying $2q - 3 \geq p$. For each $M \in \mathcal{M}_{h,i}$, we let \hat{x}_μ^M denote the μ -th quadrature point, with $\hat{x}_1^M = x_{M,l}, \hat{x}_q^M = x_{M,r}$. Here $x_{M,l}, x_{M,r}$ are the end points of I_M , the part of the macro-element, which is in the subdomain Ω_i . The corresponding weights, normalized to a unit interval, are denoted by $\hat{w}_\mu, \mu = 1, \dots, q$. We note that the weights in the chosen quadrature rules are symmetric, $\hat{w}_1 = \hat{w}_q$. We also note that after the reconstruction our approximation is a polynomial of degree p on the entire macro-element, which can be integrated exactly by the quadrature rule. The following theorem shows that one Euler step preserves the maximum principle for mean values defined by $\bar{u}_h^n = (\bar{u}_{h,1}^n, \dots, \bar{u}_{h,N_\Omega}^n)$ with

$$\bar{u}_{h,i}^n|_M = \frac{1}{|I_M|} \int_{I_M} u_{h,i}^{M,n} dx = \frac{1}{|I_M|} \int_{I_M} u_{h,i}^n dx, \quad \bar{u}_{h,i}^{M,n} = \bar{u}_{h,i}^n|_M, \quad (3.17)$$

for each macro-element $M \in \mathcal{M}_{h,i}$.

Theorem 3.2. *Consider the Cut-DG scheme described by (3.1)-(3.3) with $p \geq 1$. If the time step Δt satisfies*

$$\frac{\Delta t}{\delta h} \lambda \leq \hat{w}_1, \quad (3.18)$$

then $u_{h,i}^n|_{\Omega_i} \in [\mathfrak{m}, \mathfrak{M}], i = 1, \dots, N_\Omega$ implies that $\bar{u}_{h,i}^{M,n+1}|_{\Omega_i} \in [\mathfrak{m}, \mathfrak{M}], i = 1, \dots, N_\Omega$, that is, mean values on all macro-elements satisfy the maximum principle. Here h is the element size in the background mesh, and δ is a given constant, which in (2.8) defines when an intersection between an element and Ω_i is classified as large. λ is the maximum absolute value of the Jacobian $\partial f(u_h^n)/\partial u_h^n$ in the domain Ω . \hat{w}_1 is the normalized weight corresponding to the first interior point for a q -point Gauss-Lobatto rules with $2q - 3 \geq p$.

Proof. As in Section 3.1, we look at a macro-element M as shown in Figure 3, with $I_M = K_1 \cup K_2$. Let $u_{h,l}^n$ and $u_{h,r}^n$ denote the values adjacent to the left and right end of I_M , respectively, and let \hat{f}_r and \hat{f}_l be the corresponding numerical fluxes defined by (2.13), which is expressed in (3.6)-(3.7) on the macro-element. By reconstruction, u_h^n is a single polynomial of degree p in M , and can be exactly integrated over I_M by the q -point Gauss-Lobatto quadrature rule. Let the test function v_h in (3.1) be 1 on each element of M and 0 otherwise, to obtain

$$\sum_{j \in N_M} \int_{K_j} \tilde{u}_{h,j}^{n+1} dx = \sum_{j \in N_M} \int_{K_j} u_{h,i}^n dx - (\hat{f}_r - \hat{f}_l). \quad (3.19)$$

By conservation on macro-elements and the definition (3.2), (3.17), we have

$$\bar{u}_{h,i}^{M,n+1} = \bar{u}_{h,i}^{M,n} - \frac{\Delta t}{|I_M|} (\hat{f}_r - \hat{f}_l). \quad (3.20)$$

Applying a q -point Gauss-Lobatto quadrature rules gives

$$\bar{u}_{h,i}^{M,n} = \frac{1}{|I_M|} \int_{I_M} u_{h,i}^{M,n} dx = \sum_{\mu=1}^q \hat{w}_\mu \hat{u}_\mu^{M,n}. \quad (3.21)$$

Here $\hat{u}_\mu^{M,n} = u_{h,i}^{M,n}(\hat{x}_\mu^M)$ denotes the value of the local polynomial at the quadrature point \hat{x}_μ^M . We now follow the idea of the proof of the bound preserving property of the standard DG method for hyperbolic conservation laws, see Theorem 2.2 in [52]. But we consider the mean values $\bar{u}_{h,i}^{M,n+1}$ of the Cut-DG method on each macro-element. Introduce \hat{F} as the Lax-Friedrichs flux based on $\hat{u}_{M,1}^n$ and $\hat{u}_{M,q}^n$, that is

$$\hat{F} = \frac{1}{2}(f(\hat{u}_1^{M,n}) + f(\hat{u}_q^{M,n})) - \frac{\lambda}{2}(\hat{u}_q^{M,n} - \hat{u}_1^{M,n}), \quad (3.22)$$

Using the quadrature (3.21), $\hat{\omega}_1 = \hat{\omega}_q$ and the definition of $H(a, b, c; \lambda)$ in (3.10), the equation (3.20) can be rewritten as

$$\begin{aligned} \bar{u}_{h,i}^{M,n+1} &= \sum_{\mu=1}^q \hat{w}_\mu \hat{u}_\mu^{M,n} - \frac{\Delta t}{|I_M|} (\hat{f}_r - \hat{f}_l) = \\ &= \sum_{\mu=2}^{q-1} \hat{w}_\mu \hat{u}_\mu^{M,n} + \hat{w}_1 \left(\hat{u}_1^{M,n} - \frac{\Delta t}{\hat{w}_1 |I_M|} (\hat{F} - \hat{f}_l) \right) + \hat{w}_q \left(\hat{u}_q^{M,n} - \frac{\Delta t}{\hat{w}_q |I_M|} (\hat{f}_r - \hat{F}) \right) = \\ &= \sum_{\mu=2}^{q-1} \hat{w}_\mu \hat{u}_\mu^{M,n} + \hat{w}_1 H(\hat{u}_0^{M,n}, \hat{u}_1^{M,n}, \hat{u}_q^{M,n}; \lambda/\hat{w}_1) + \hat{w}_q H(\hat{u}_1^{M,n}, \hat{u}_q^{M,n}, \hat{u}_{q+1}^{M,n}; \lambda/\hat{w}_q). \end{aligned}$$

Here $\hat{u}_0^{M,n} = u_{h,l}^n(x_{M,l})$ and $\hat{u}_{q+1}^{M,n} = u_{h,r}^n(x_{M,r})$ are used. We can see that the above expression is a linear combination of two first order schemes (3.11) and $\sum_{\mu=2}^{q-1} \hat{w}_\mu \hat{u}_\mu^{M,n}$. As in Theorem 3.1, we can conclude that $\bar{u}_{h,i}^{M,n+1} \in [\mathfrak{m}, \mathfrak{M}]$ under the condition $\frac{\Delta t}{\delta h} \lambda \leq \hat{w}_1$. \square

We note that the time restrictions in (3.5) and (3.18) are of the same order as for the corresponding standard DG methods on the background grid. When we set $\delta = 1$, the time-step restrictions are same as in the standard un-cut case, but all cut elements are stabilized.

3.3 A bound preserving limiter for scalar problems

In our proposed scheme described in (3.1)-(3.3) and in Theorems 3.1-3.2, we require $u_{h,i}^n|_{\Omega_i} \in [\mathfrak{m}, \mathfrak{M}]$, $i = 1, \dots, \Omega_N$, but the high order reconstructed solution at next time level may not satisfy this requirement. In order to guarantee that the solution remains within the bounds at later times, we use a bound preserving limiter developed by Zhang and Shu [52] for high order approximations. In the standard DG method, the solution $u_h(x)$ is modified locally in each element I such that mean values are un-changed, and $u_h(x) \in [\mathfrak{m}, \mathfrak{M}]$ for $x \in S_I$, where S_I is set of the Gauss-Lobatto quadrature points on I . In the unfitted case, a cut element I may be such that $I \cap \Omega_i$ is very small but $I_M = M \cap \Omega_i$ is always large. Therefore we propose to apply the limiter to the reconstructed solution in each macro-element M . For each macro-element M we define the limited solution $u_{h,i}^{M,(l)}(x)$ by

$$u_{h,i}^{M,(l)}(x) = \theta (u_{h,i}^M(x) - \bar{u}_{h,i}^M) + \bar{u}_{h,i}^M, \quad \theta = \min \left\{ \left| \frac{\mathfrak{M} - \bar{u}_{h,i}^M}{\mathfrak{M}_M - \bar{u}_{h,i}^M} \right|, \left| \frac{\mathfrak{m} - \bar{u}_{h,i}^M}{\mathfrak{m}_M - \bar{u}_{h,i}^M} \right|, 1 \right\}. \quad (3.23)$$

Here we assume $u_{h,i}^M$ is a reconstructed solution on M and

$$\mathbf{M}_M = \max_{x \in I_M} u_{h,i}^M(x), \quad \mathbf{m}_M = \min_{x \in I_M} u_{h,i}^M(x). \quad (3.24)$$

Then, we let $u_{h,i}^{\mathcal{M}}|_M = u_{h,i}^{M,(l)}(x)$, which satisfies the maximum principle on Ω_i . As for the standard DG method, we can use $u_{h,i}^{M,(l)}(x)$ instead of $u_{h,i}^M(x)$ without destroying the accuracy. We note that the exact minimum value and maximum value of the polynomials is needed on the macro-element.

By combining the sequence of steps (3.1)-(3.3) with (3.23), we can get a fully discrete, bound preserving scheme for scalar problems for any polynomial order. For clarity we have formulated the version based on a third order Runge-Kutta discretization (5.2) in time in Algorithm 1.

Algorithm 1: Fully discrete bound preserving Cut-DG method for scalar problem

Data: Given initial condition $u_0(x)$ at $t = 0$
Result: Bound preserving approximation at final time T

- 1 Initialize \tilde{u}_h^0 by (2.14) and $n = 0$;
- 2 $u_h^0 = \text{Reconstruction and limiting}(\tilde{u}_h^0)$;
- 3 **while** $t \leq T$ **do**
- 4 Compute suitable time-step Δt based on Theorem 3.1/3.2;
- 5 /* Runge-Kutta time discretization */
- 6 $\tilde{u}_h^{(1)} = \text{Euler-Step}(u_h^n, t_n, \Delta t)$; // first stage
- 7 $u_h^{(1)} = \text{Reconstruction and limiting}(\tilde{u}_h^{(1)})$;
- 8 $u_h^{(2')} = \text{Euler-Step}(u_h^{(1)}, t_n + \Delta t, \Delta t)$; // second stage
- 9 Set: $\tilde{u}_h^{(2)} = \frac{3}{4}u_h^n + \frac{1}{4}u_h^{(2')}$;
- 10 $u_h^{(2)} = \text{Reconstruction and limiting}(\tilde{u}_h^{(2)})$;
- 11 $\tilde{u}_h^{(3')} = \text{Euler-Step}(u_h^{(2)}, t_n + \Delta t/2, \Delta t)$; // third stage
- 12 Set: $\tilde{u}_h^{(3)} = \frac{1}{3}u_h^n + \frac{2}{3}u_h^{(3')}$;
- 13 $u_h^{(3)} = \text{Reconstruction and limiting}(\tilde{u}_h^{(3)})$;
- 14 Set: $u_h^{n+1} = u_h^{(3)}$;
- 15 $n \leftarrow n + 1$;
- 16 $t \leftarrow t + \Delta t$;
- 17 **end**
- 18 **Function Euler-step**($u_h, t, \Delta t$)
- 19 Using (3.1) with $u_h, t, \Delta t$ to get $\tilde{u}_h = (\tilde{u}_{h,1}, \tilde{u}_{h,2}, \dots, \tilde{u}_{h,N_\Omega}) \in V_h^p$;
- 20 **return** $\tilde{u}_h = (\tilde{u}_{h,1}, \tilde{u}_{h,2}, \dots, \tilde{u}_{h,N_\Omega})$;
- 21 **Function Reconstruction and limiting**(\tilde{u}_h)
- 22 **for** $i = 1$ **to** N_Ω **do**
- 23 Using (3.2) with \tilde{u}_h to reconstruct $u_{h,i}^{\mathcal{M}}, i = 1, \dots, N_\Omega$;
- 24 **if** $u_{h,i}^{\mathcal{M}}|_{\Omega_i} \notin [\mathbf{m}, \mathbf{M}]$ **then** modify $u_{h,i}^{\mathcal{M}}$ by (3.23);
- 25 $u_{h,i} \leftarrow u_{h,i}^{\mathcal{M}}$;
- 26 **end**
- 27 **return** $u_h = (u_{h,1}, u_{h,2}, \dots, u_{h,N_\Omega}) \in V_h^p$;

4 A Positivity preserving Cut-DG method for the Euler equations

In this section, we will show how the positivity property for the Euler equations can be built into our proposed Cut-DG method. The Euler equations in one space dimension are

$$\mathbf{u}_t + \partial_x \mathbf{f}(\mathbf{u}) = 0, \quad t \geq 0, x \in \Omega \subset \mathbb{R}, \quad (4.1)$$

$$\mathbf{u} = \begin{pmatrix} \rho \\ m \\ E \end{pmatrix}, \quad \mathbf{f}(\mathbf{u}) = \begin{pmatrix} m \\ \rho u^2 + p \\ (E + p)u \end{pmatrix}. \quad (4.2)$$

Here ρ is the density, m the momentum, and E the total energy. These quantities are often called the conservative variables, and are related to other physical quantities such as the velocity u , the pressure p , and the internal energy e through $E = \frac{1}{2}\rho u^2 + \rho e$, $m = \rho u$, and $p = (\gamma - 1)\rho e$. Here γ is the specific gas constant. Note that the pressure p can be written as a function of the conservative variables,

$$p(\mathbf{u}) = (\gamma - 1) \left(E - \frac{1}{2} \frac{m^2}{\rho} \right). \quad (4.3)$$

Also important is the sound speed, given by $c = \sqrt{\gamma p / \rho}$.

In physically relevant solutions, the density and pressure should be positive. Without positivity hyperbolicity is lost, and the mathematical problem is ill-posed. If the solution is initially positive, it can be proven that the solution of the compressible Euler equations cannot lose positivity of density and pressure, see [22, 15, 8]. Therefore we define the following set

$$G = \left\{ \mathbf{u} = (\rho, m, E)^T \mid \rho > 0, p(\mathbf{u}) = (\gamma - 1) \left(E - \frac{1}{2} \frac{m^2}{\rho} \right) > 0 \right\}, \quad (4.4)$$

as the set of admissible solutions for the compressible Euler equations (4.1). Since $-p(\mathbf{u})$ is convex, we have using Jensen's inequality for any $0 \leq s \leq 1$, $\mathbf{u}_1 = (\rho_1, m_1, E_1)^T \in G$, and $\mathbf{u}_2 = (\rho_2, m_2, E_2)^T \in G$ we have

$$p(s\mathbf{u}_1 + (1-s)\mathbf{u}_2) \geq sp(\mathbf{u}_1) + (1-s)p(\mathbf{u}_2) > 0, \quad \text{if } \rho_1 \geq 0, \rho_2 \geq 0. \quad (4.5)$$

Thus G is a convex set.

Numerical methods that do not preserve the positivity property, may cause numerical instability or nonphysical features in approximated solutions of problems with low density, or high Mach number [25]. Preserving positivity of pressure and density is therefore an important property of a numerical method for the Euler equations, and it can be seen as a generalization of the maximum principle for scalar conservation laws. As for the scalar problems, we will be working with mean values on macro-element $M \in \mathcal{M}_{h,i}, i = 1, \dots, N_\Omega$. For each component of \mathbf{u}_h , we define the mean values on the macro-element M as in (3.17), and for the pressure we define $\bar{p}_{h,i}^M := p(\bar{\mathbf{u}}_{h,i}^M) = (\gamma - 1) \left(\bar{E}_{h,i}^M - \frac{1}{2} (\bar{m}_h, i^M)^2 / \bar{\rho}_{h,i}^M \right)$. By $\bar{\mathbf{u}}_{h,i}^M \in G$ we mean $\bar{\rho}_{h,i}^M > 0$ and $\bar{p}_{h,i}^M > 0$.

4.1 Piecewise constant approximations

In this subsection, we will study the piecewise constant scheme, (3.1)-(3.3), for the compressible Euler equations (4.1). We are particularly interested in the positivity property, which was discussed above. For the piecewise constant method we prove the following positivity result.

Theorem 4.1. Consider the piecewise constant Cut-DG scheme described by (3.1)-(3.3) applied to the Euler equations (4.1). The reconstruction (3.2) is done component wise. If the time step Δt satisfies

$$\frac{\Delta t}{\delta h} \lambda \leq 1, \quad (4.6)$$

then $\mathbf{u}_{h,i}^n|_{\Omega_i} \in G, i = 1, \dots, N_\Omega$ implies $\mathbf{u}_{h,i}^{n+1}|_{\Omega_i} \in G, i = 1, \dots, N_\Omega$. Here h is the element size in the background mesh, and δ is a given constant, which in (2.8) defines when an intersection between an element and Ω_i is classified as large. $\lambda = \max_{x \in \Omega} |u| + c$ is the largest absolute eigenvalue of Jacobian matrix $\frac{\partial \mathbf{f}(\mathbf{u}_h^n)}{\partial \mathbf{u}_h^n}$ in the entire domain Ω .

Proof. As before we consider each macro-element $M \in \mathcal{M}_{h,i}, i = 1, \dots, N_\Omega$ separately. Let $\mathbf{u}_{h,l}^n = (\rho_{h,l}^n, m_{h,l}^n, E_{h,l}^n)$, $\mathbf{u}_{h,r}^n = (\rho_{h,r}^n, m_{h,r}^n, E_{h,r}^n)$, $\mathbf{u}_{h,i}^{M,n}$ denote the solution on the left side and right side of I_M , and in I_M , respectively. By assumption $\mathbf{u}_{h,l}^n, \mathbf{u}_{h,i}^{M,n}, \mathbf{u}_{h,r}^n \in G$, and $\mathbf{u}_{h,i}^{M,n}$ is constant in I_M . Following the same analysis as for the scalar conservation law, we get

$$\mathbf{u}_{h,i}^{M,n+1} = \mathbf{H}(\mathbf{u}_{h,l}^n, \mathbf{u}_{h,i}^{M,n}, \mathbf{u}_{h,r}^n; \lambda), \quad (4.7)$$

$$\mathbf{H}(\mathbf{u}_{h,l}^n, \mathbf{u}_{h,i}^{M,n}, \mathbf{u}_{h,r}^n; \lambda) := \mathbf{u}_{h,i}^{M,n} - \frac{\Delta t}{|I_M|} (\hat{\mathbf{f}}_r - \hat{\mathbf{f}}_l). \quad (4.8)$$

Here $\hat{\mathbf{f}}_r$ and $\hat{\mathbf{f}}_l$ are the numerical fluxes on the right and the left edge of I_M , respectively. We use the global Lax-Friedrichs flux (2.13) with $\lambda = \max_{x \in \Omega} \{|u| + c\}$, which is the largest absolute value of eigenvalues of the Jacobian matrix $\frac{\partial \mathbf{f}(\mathbf{u}_h^n)}{\partial \mathbf{u}_h^n}$. Next, we study the positivity property for the density and pressure of (4.7). From the definition of the global Lax-Friedrichs flux (2.13) applied to the particular Euler flux (4.2) we have

$$\begin{aligned} \rho_{h,i}^{M,n+1} &= \rho_{h,i}^{M,n} - \frac{\Delta t}{2|I_M|} (m_{h,i}^{M,n} + m_{h,r}^n - \lambda(\rho_{h,r}^n - \rho_{h,i}^{M,n})) + \frac{\Delta t}{2|I_M|} (m_{h,i}^{M,n} + m_{h,l}^n - \lambda(\rho_{h,i}^{M,n} - \rho_{h,l}^n)) \\ &= \left(1 - \frac{\Delta t}{|I_M|} \lambda\right) \rho_{h,i}^{M,n} + \frac{\Delta t}{2|I_M|} \rho_{h,r}^n (\lambda - u_{h,r}^n) + \frac{\Delta t}{2|I_M|} \rho_{h,l}^n (\lambda + u_{h,l}^n). \end{aligned} \quad (4.9)$$

From $\lambda = \max_{x \in \Omega} |u| + c$ it follows that $\lambda \pm u \geq 0$, and since $|I_M| \geq \delta h$ and

$$\rho_{h,i}^{M,n} > 0, \rho_{h,l}^n > 0, \rho_{h,r}^n > 0, \quad 1 - \frac{\lambda \Delta t}{|I_M|} > 0, \quad (4.10)$$

we conclude from equation (4.9) that $\rho_{h,i}^{M,n+1} > 0$ under time step restriction (4.6). To show that $\mathbf{u}_{h,i}^{M,n+1} \in G$ it remains to consider the pressure that corresponds to $\mathbf{u}_{h,i}^{M,n+1}$. Following the analysis in [20], we define $V_a(\mathbf{u}_{h,l}^n) = \mathbf{f}(\mathbf{u}_{h,l}^n)/\lambda + \mathbf{u}_{h,l}^n$ and $V_b(\mathbf{u}_{h,r}^n) = \mathbf{u}_{h,r}^n - \mathbf{f}(\mathbf{u}_{h,r}^n)/\lambda$, and rewrite (4.8) as

$$\mathbf{H}(\mathbf{u}_{h,l}^n, \mathbf{u}_{h,i}^{M,n}, \mathbf{u}_{h,r}^n; \lambda) = \left(1 - \frac{\lambda \Delta t}{|I_M|}\right) \mathbf{u}_{h,i}^{M,n} + \frac{\lambda \Delta t}{2|I_M|} V_a(\mathbf{u}_{h,l}^n) + \frac{\lambda \Delta t}{2|I_M|} V_b(\mathbf{u}_{h,r}^n). \quad (4.11)$$

As in [20] (see Lemma 3.1), we have $p(V_a) > 0$ and $p(V_b) > 0$ if $\mathbf{u}_{h,l}^n, \mathbf{u}_{h,r}^n \in G$. By the convexity of G we obtain the desired result. We refer to the corresponding analysis for the DG method on a non-cut mesh in [53] and [20] for more details. \square

4.2 Mean values for higher order approximations

Next we consider high order schemes, where as before the time discretization can be seen as a sequence of Euler steps. We therefore consider (3.1) with $p \geq 1$ together with the reconstruction in (3.2)-(3.3). Similarly to the scalar case we show a sufficient condition for the mean values on each macro-element to satisfy the positivity property. We again use the q -point Gauss-Lobatto quadrature rule on each macro element, with $2q - 3 \geq p$. We will prove the following theorem.

Theorem 4.2. Consider (3.1)-(3.3) with $p \geq 1$ for the Euler equations (4.1), and with the reconstruction done component-wise. If the time step Δt satisfies

$$\frac{\Delta t}{\delta h} \lambda \leq \hat{w}_1, \quad (4.12)$$

then $\mathbf{u}_{h,i}^n|_{\Omega_i} \in G, i = 1, \dots, N_\Omega$ implies that the mean value on each macro element satisfies $\bar{\mathbf{u}}_{h,i}^{M,n+1}|_{\Omega_i} \in G$ for $i = 1, \dots, N_\Omega$. Here h is the element size in the background mesh, and δ is a given constant, which in (2.8) defines when an intersection between an element and Ω_i is classified as large. λ denotes the largest absolute value of the Jacobian matrix $\partial \mathbf{f}(\mathbf{u}_h^n) / \partial \mathbf{u}_h^n$ in the entire domain Ω . Further \hat{w}_1 is the normalized quadrature weight corresponding to the first quadrature point of a q -point Gauss-Lobatto quadrature rule with $2q - 3 \geq p$.

Proof. Similar to the high order Cut-DG scheme (3.20) for scalar problems, we have for the mean values of the reconstructed approximation on I_M in (2.15) that

$$\bar{\mathbf{u}}_{h,i}^{M,n+1} = \bar{\mathbf{u}}_{h,i}^{M,n} - \frac{\Delta t}{|I_M|} (\hat{\mathbf{f}}_r - \hat{\mathbf{f}}_l). \quad (4.13)$$

We will now show that $\bar{\mathbf{u}}_{h,i}^{M,n+1} \in G$. We introduce the Gauss-Lobatto quadrature to decompose the mean values on each macro-element, see (3.21), and rewrite (4.13) as

$$\begin{aligned} \bar{\mathbf{u}}_{h,i}^{M,n+1} &= \sum_{\mu=1}^q \hat{w}_\mu \hat{\mathbf{u}}_\mu^{M,n} - \frac{\Delta t}{|I_M|} (\hat{\mathbf{f}}_r - \hat{\mathbf{f}}_l) = \\ &= \sum_{\mu=2}^{q-1} \hat{w}_\mu \hat{\mathbf{u}}_\mu^{M,n} + \hat{w}_1 \mathbf{H}(\hat{\mathbf{u}}_0^{M,n}, \hat{\mathbf{u}}_1^{M,n}, \hat{\mathbf{u}}_q^{M,n}; \frac{\lambda}{\hat{w}_1}) + \hat{w}_q \mathbf{H}(\hat{\mathbf{u}}_1^{M,n}, \hat{\mathbf{u}}_q^{M,n}, \hat{\mathbf{u}}_{q+1}^{M,n}; \frac{\lambda}{\hat{w}_q}). \end{aligned}$$

Here $\hat{\mathbf{u}}_0^{M,n} = \mathbf{u}_{h,l}^n(x_{M,l})$ and $\hat{\mathbf{u}}_{q+1}^{M,n} = \mathbf{u}_{h,r}^n(x_{M,r})$ denote the approximations from the left side and right side of I_M , respectively. With the positivity-property of the piecewise constant scheme (4.7) and time step restriction (4.12), it follows that $\frac{\Delta t}{|I_M|} \lambda \leq \hat{w}_1$ implies $\mathbf{H}(\hat{\mathbf{u}}_0^{M,n}, \hat{\mathbf{u}}_1^{M,n}, \hat{\mathbf{u}}_q^{M,n}; \frac{\lambda}{\hat{w}_1}) \in G$ and $\mathbf{H}(\hat{\mathbf{u}}_1^{M,n}, \hat{\mathbf{u}}_q^{M,n}, \hat{\mathbf{u}}_{q+1}^{M,n}; \frac{\lambda}{\hat{w}_q}) \in G$. Thus, we get $\bar{\mathbf{u}}_{h,i}^{M,n+1} \in G$ since $\bar{\mathbf{u}}_{h,i}^{M,n+1}$ is a convex combination of solutions in G . \square

4.3 Positivity preserving limiting for the Euler equations

As for the standard DG method for the Euler equations on a non-cut mesh, we need to apply a positivity preserving limiter to ensure the positivity of density and pressure for $p \geq 1$. We will use the limiter developed by Zhang and Shu [53], which is briefly introduced below. It retains conservation everywhere, and accuracy in smooth regions. We will apply it to the reconstructed solution in each inner stage of each time step. By the previous theorem, we know that mean values on all macro-elements are in G . Let $M \in \mathcal{M}_{h,i}$ represent a macro-element in Ω_i and $\mathbf{u}_h^M = (\rho_h^M, m_h^M, E_h^M)$ denote the corresponding solution on the macro-element M . By the previous theorem $\bar{\rho}_h^M > 0$ and $\bar{p}_h^M > 0$. We assume there exists a small number $\varepsilon > 0$ such that $\bar{\rho}_h^M \geq \varepsilon$ and $\bar{p}_h^M \geq \varepsilon$ for all macro-elements. In our computation, we take $\varepsilon = 10^{-8}$. We first limit the density by replacing $\rho_h^M(x)$ by $\rho_h^{M,(l)}(x)$

$$\rho_h^{M,(l)}(x) = \theta_1 (\rho_h^M(x) - \bar{\rho}_h^M) + \bar{\rho}_h^M, \quad (4.14)$$

where

$$\theta_1 = \min \left\{ \frac{\bar{\rho}_h^M - \varepsilon}{\bar{\rho}_h^M - \rho_{\min}}, 1 \right\}, \quad \rho_{\min} = \min_k \rho_h^M(\hat{x}_\mu^M). \quad (4.15)$$

Then, let $\widehat{\mathbf{q}}_h^M(x) = \left(\rho_h^{M,(l)}(x), m_h^M(x), E_h^M(x) \right)^T$ and denote $\widehat{\mathbf{q}}_h^M(\widehat{x}_\mu^M)$ by $\widehat{\mathbf{q}}_\mu^M$. Next, $\widehat{\mathbf{q}}_h^M$ is limited to enforce the positivity of the pressure. Define

$$G^\varepsilon = \{ \mathbf{u} = (\rho, m, E)^T \mid \rho \geq \varepsilon \text{ and } p \geq \varepsilon \}, \quad \partial G^\varepsilon = \{ \mathbf{u} = (\rho, m, E)^T \mid \rho \geq \varepsilon \text{ and } p = \varepsilon \}, \quad (4.16)$$

and

$$\mathbf{s}^\mu(t) = (1-t)\overline{\mathbf{u}}_h^{M,n} + t\widehat{\mathbf{q}}_h^M(\widehat{x}_\mu^M), \quad 0 \leq t \leq 1. \quad (4.17)$$

Let $\mathbf{s}_\varepsilon^\mu$ be solution of $p(\mathbf{s}^\mu(t_\varepsilon^k)) = \varepsilon$ when $p(\widehat{\mathbf{q}}_\mu^M) < \varepsilon$, and $\mathbf{s}_\varepsilon^\mu = \widehat{\mathbf{q}}_\mu^M$ if $p(\widehat{\mathbf{q}}_\mu^M) \in G^\varepsilon$. Finally, we modify the solution by

$$\mathbf{u}_h^{M,(l)}(x) = \theta_2 (\widehat{\mathbf{q}}_h^M(x) - \overline{\mathbf{u}}_h^M) + \overline{\mathbf{u}}_h^M, \quad \theta_2 = \min_{\mu=1,2,\dots,q} \mathbf{s}_\varepsilon^\mu. \quad (4.18)$$

We note that it is hard to find the exact minimum value θ_2 on the cut mesh. We use the Gauss-Lobatto points on the macro-element and on each element intersection Ω_i involved in the macro-element M . Finally, we set $\mathbf{u}_{h,i}^{M,n}|_{\Omega_i} = \mathbf{u}_h^{M,(l)}(x)$ on the macro-element M .

For clarity, we formulate our proposed positivity preserving Cut-DG method for the Euler equations in Algorithm 2 in the Appendix.

5 Numerical results

In this section we present some numerical examples that verify the bound preserving properties of our proposed bound preserving Cut-DG scheme, which includes reconstruction on macro-elements and applying bound preserving limiters. In all the Cut-DG computations we use a uniform mesh with N elements as the background mesh and $N \geq 4$. We assume we have $N/4$ subdomains interfaces, which cut $N/4$ elements in the middle part of the domain. Each interface cuts an element into two pieces with size $\alpha_k h$ and $1 - \alpha_k h$, respectively, where α is fixed and

$$\alpha_k = s\alpha, \quad s \in [10^{-6}, 1] \text{ is a random number.} \quad (5.1)$$

Thus we have $N/4 + 1$ subdomains. The parameters in the stabilization (see (2.12)) and in (2.8) are set to $\gamma_1 = 0.75, \gamma_0 = 0.25, \omega_k = 1/(k!)^2$, and $\delta = 0.2$, respectively.

Two different high order strong stability preserving (SSP) methods are as time discretization. To define the methods consider $u_t = L(u)$, where $L(u)$ is the spatial operator. The first method is the third order Runge-Kutta method, which is convex combinations of the forward Euler method

$$u^{(1)} = u^n + \Delta t L(u^n) \quad (5.2)$$

$$u^{(2)} = \frac{3}{4}u^n + \frac{1}{4}u^{(1)} + \frac{4}{\Delta}tL(u^{(1)}), \quad (5.3)$$

$$u^{n+1} = \frac{1}{3}u^n + \frac{2}{3}u^{(2)} + \frac{2\Delta t}{3}L(u^{(2)}). \quad (5.4)$$

The second scheme is the third order multi-step time discretization [23]

$$u^{n+1} = \frac{16}{27}(u^n + 3\Delta t L(u^n)) + \frac{11}{27}\left(u^{n-3} + \frac{12}{11}\Delta t L(u^{n-3})\right). \quad (5.5)$$

By the pervious analysis each time step and interior stage will be bound preserving if the time step is sufficiently restricted. It follows that the proposed strategy, with both time discretizations, will satisfy

the maximum principle or positivity of density and pressure. In the next section, we compute the two time discretization schemes and show that optimal accuracy is obtained with third order multi-step time discretizations. We note that we use P^p with $p = 1, 2, 3$ to denote the space of piecewise p -th degree polynomials V_h^p .

5.1 Scalar linear case

In this subsection, we solve the one dimensional linear advection equation with periodic boundary condition

$$u_t + u_x = 0, t > 0, \quad (5.6)$$

together with smooth and non-smooth initial data, respectively.

5.1.1 Accuracy test with smooth initial data

We first use our proposed bound preserving Cut-DG method (3.1)-(3.3) together with the bound preserving limiter in (3.23) to solve (5.6), with smooth initial data $u(x, 0) = 1.0 + 0.5 \sin(\pi x)$ in the domain $[0, 2]$. The exact solution is $u(x, t) = 1 + 0.5 \sin(\pi(x-t))$. The problem is solved on a mesh where the elements in interval $[0.75, 1.25]$ are cut. In our test, we use $\alpha = 0.1$ in (5.1) with $N = 20, 40, 80, 160, 320, 640$. Other alpha values have also been tested, with similar results (and therefore not reported here). We first solve the problem using the third order SSP-RK method (5.2) and the time step is taken to be $\Delta t = Ch$ for second and third order approximations and $\Delta t = Ch^{4/3}$ for fourth order approximations, where $C = 0.5(1 - \max(\alpha_k))\hat{w}_1$. Here $h^{4/3}$ is used for P^3 approximations to balance the errors caused by time and space discretization, and \hat{w}_1 is the weight used in the Gauss-Lobatto quadrature. The results at $t = 1$ are shown in Figure 4. We can observe that the Cut-DG method using the third Runge-Kutta method and the bound preserving limiter has accuracy degeneracy. This is also the case for the standard DG method with Runge-Kutta time discretization [52]. When the third order multi-step method (5.5) is applied with $\Delta t = h/24, h^{4/3}/15$ for P^2, P^3 approximation, the optimal accuracy is obtained, see the right panel of Figure 4. The results verify that the reconstruction of solutions and the bound preserving limiter on macro-elements in our proposed method can keep the same high order accuracy as the standard Cut-DG method [19, 18]. The results also show that the proposed scheme enforce the maximum principle.

5.1.2 Non-smooth initial data

Here, we solve the advection problem (5.6) with periodic boundary condition on the domain $\Omega = [0, 1]$ and non-smooth initial data

$$u(x, 0) = \begin{cases} 1 & 0.1 < x < 0.5, \\ 0 & \text{otherwise.} \end{cases} \quad (5.7)$$

We use a computational mesh, where the elements in the interval $[0.375, 0.625]$ are cut. In particular we note that the discontinuity is initially located on the common edge of one cut element and its neighbour. We first solve this problem using the cut DG discretization (2.9) with $p = 1, 2$, but without reconstruction and without any bound preserving limiter. We observe overshoots and undershoots of the solution near the discontinuities, see the left panel of Figure 5. In the middle panel of Figure 5, we show the results when the bound preserving limiter (3.23) is applied to the solution on each element. A clear overshoot still exists in the second order approximations, which will decrease with increasing degree of the polynomials. We point out that we still observe overshoots or undershoots during time evolution in the P^2, P^3 approximations but they are quite small and decrease with time. The results from our proposed Cut-DG method with bound

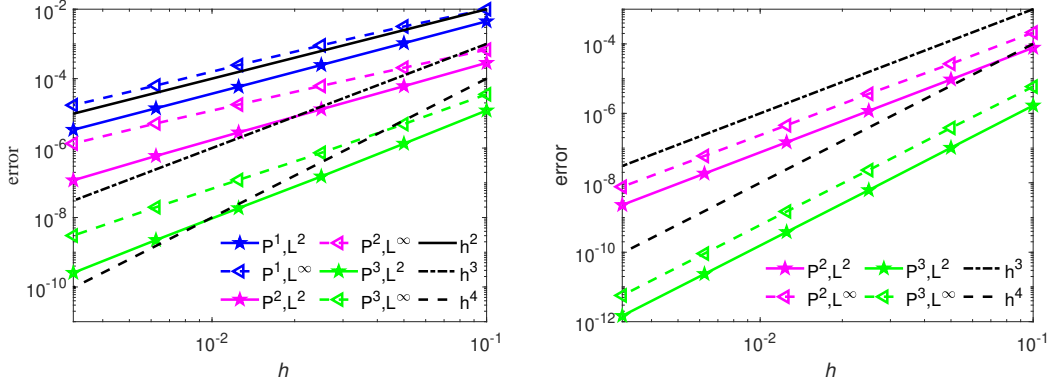


Figure 4: The errors in the numerical solutions for the advection equation with smooth initial data at $t = 1.0$. Errors are shown in both the L^2 -norm (solid lines) and L^∞ -norm (dashed lines). Left: time discretization using third order Runge-Kutta method. Right: time discretization using third order multi-step discretization in (5.5).

preserving limiter (3.23) and reconstruction (3.2) on the macro-elements are shown in the right panel of Figure 5. We did not observe any overshoots or undershoots up to the final time. We also solved this problem on a mesh where the cut elements are randomly located and have different cut sizes, with similar results.

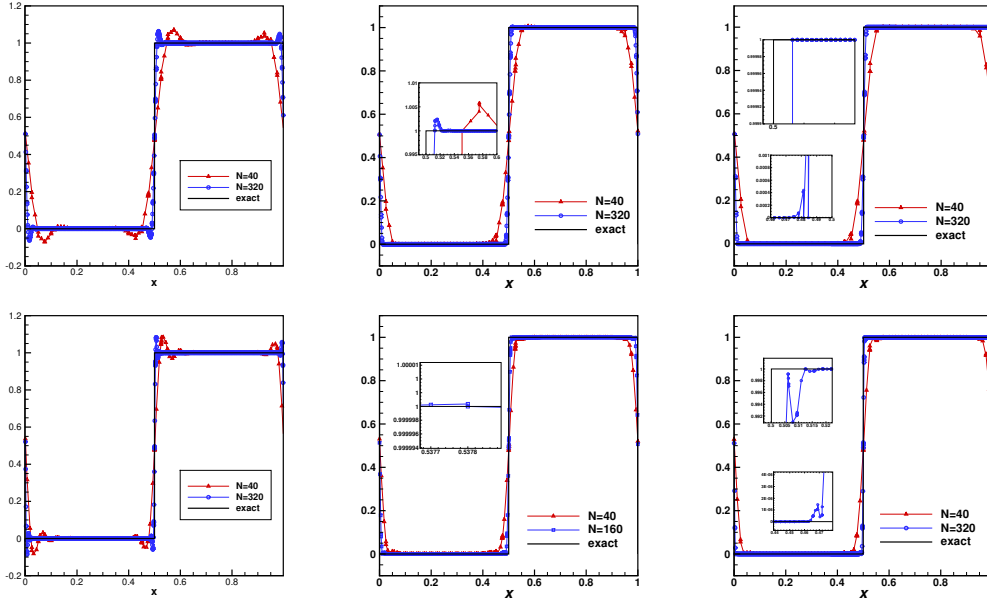


Figure 5: Numerical P^1 (top), P^2 (bottom) solutions for the advection equation with non-smooth initial data at $t = 1.0$. Left: without reconstruction and without limiter. Middle: without reconstruction but limiter (3.23) is applied. Right: solution with reconstruction and limiter (3.23) applied on macro-elements.

5.2 Burgers' equation

In this subsection, we consider the Burgers' equation

$$u_t + \left(\frac{u^2}{2}\right)_x = 0, \quad t > 0, \quad (5.8)$$

together with different initial data and suitable boundary conditions.

5.2.1 Smooth initial data

We first solve the Burgers' equation (5.8) with smooth initial data $u_0(x) = \sin(\pi x)$, $x \in [0, 2]$ and periodic boundary condition. This problem has a known solution, which we use as a reference when computing errors. The solution is initially smooth, but at $t = \frac{1}{\pi}$ a shock forms at $x = 1$. We compute until time $t = 0.2$, which is before the shock appears. Uniform meshes with $N = 20, 40, 80, 160, 320, 640$ elements are used as background mesh. The cut elements are located in $[0.75, 1.25]$. The third order multi-step (5.5) is used for time discretization. In Figure 6, the L^2 and L^∞ errors are shown from our proposed bound preserving Cut-DG scheme. We observe the third and fourth order accuracy for P^2, P^3 approximations, respectively.

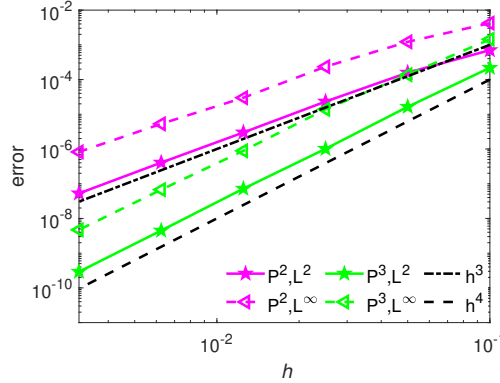


Figure 6: Errors in the numerical solution of Burgers' equation with smooth initial data, before a shock has formed. Our proposed Cut-DG method based on piecewise P^2 and P^3 approximations, with reconstruction and bound preserving limiter (3.23) was used on macro-elements.

Next we solve Burgers' equation with P^3 approximations until time $t = 0.5$, when a shock has formed. The third order RK method (5.2) is used for the time discretization to save computational cost, since multi-step methods need to save more informations on different time levels. Results for $h = 1/20, 1/320$ (corresponding to 10, 160 small cut elements) with the bound preserving limiter are shown in Figure 7. The left panel in Figure 7 shows the results from the scheme (3.1) without reconstruction but with bound preserving limiter. Note that the numerical solutions do not satisfy maximum principle. The middle panel in Figure 7 shows the results from our proposed bound preserving Cut-DG method with reconstruction on all macro-elements, which verifies our theoretical analysis. We did not observe any overshoots/undershoots at any time. Note that the proposed scheme on the fine mesh can capture the shock quite well, even though we did not apply a slope limiter. On the right side of Figure 7, we show the results from the scheme with the reconstruction (2.18) applied only on those macro-elements where the solution does not satisfy the maximum principle in an element belonging to these macro-elements. We can observe that the numerical solution still satisfies the maximum principle, even when the reconstruction is not applied on all macro-elements.

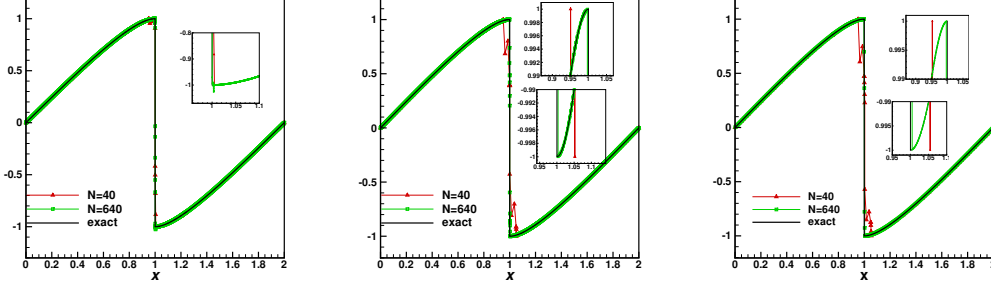


Figure 7: Numerical fourth order solutions for the Burgers' equation with smooth initial data at $t = 0.5$. Left: Basic scheme without reconstruction but with limiter. Middle: Proposed scheme including reconstruction and limiter (3.23) applied on all macro-elements. Right: Proposed scheme including reconstruction and limiter (3.23) is applied only on macro-elements, where the numerical solution does not satisfy the maximum principle on the involved elements.

5.2.2 Riemann problems

Consider Burgers' equation (5.8) on $[-2, 2]$ with initial data

$$u_0(x) = \begin{cases} u_l, & x \leq 0, \\ u_r, & x > 0. \end{cases}$$

We will use our proposed bound preserving Cut-DG scheme (3.1)-(3.3) with P^1, P^2, P^3 approximations together with the bound preserving limiter (3.23). All elements in the interval $[-0.5, 0.5]$ are cut. We solve with two sets of initial data, $u_l = -1 < 0 < u_r = 1$ and $u_l = 1 > 0 > u_r = -0.5$, respectively. Figure 8 shows the numerical solutions from the proposed bound preserving Cut-DG scheme based on $P^p, p = 1, 2, 3$ approximations, together with third order RK method (5.2) for time discretization. Our proposed scheme can simulate these two Riemann problems without violating the maximum principle. We note that violations of the maximum principle occur near the shock in the case $u_l = 1 > 0 > u_r = -0.5$, when the bound preserving limiter is applied to the basic scheme (3.1) without reconstruction.

5.3 Scalar case with discontinuous flux function

In this subsection, we consider a hyperbolic conservation law with an interface, where the flux function is discontinuous. Let

$$f(u) = H(x - x_\Gamma)h(u) + (1 - H(x - x_\Gamma))g(u), \quad x \in [-1, 1], \quad (5.9)$$

where $H(x)$ is the Heaviside function and $g(u) = u^2/2, h(u) = u$. In the example, which is taken from [1], the transport equation switches to the Burgers' equation across the interface $x = x_\Gamma$. Here, we take $x_\Gamma = 2 \cdot 10^{-5}$ and use a uniform mesh with N elements and $h = |\Omega|/N$. Thus, there is a small cut cell with size αh with $\alpha = N \cdot 10^{-5}$ in the interior of the domain. The initial condition is taken as

$$u(x, 0) = \begin{cases} 0.5 & x < -0.5, \\ 2 & \text{otherwise.} \end{cases} \quad (5.10)$$

This condition is chosen such that the Rankine-Hugoniot condition at the interface x_Γ is $[u]_\Gamma = 0$ before the discontinuity interacts with the interface, and $[f(u)]_\Gamma = 0$ afterwards. We use our proposed bound-preserving CutDG scheme with the Lax-Friedrichs flux on the interior element edges and the upwind flux

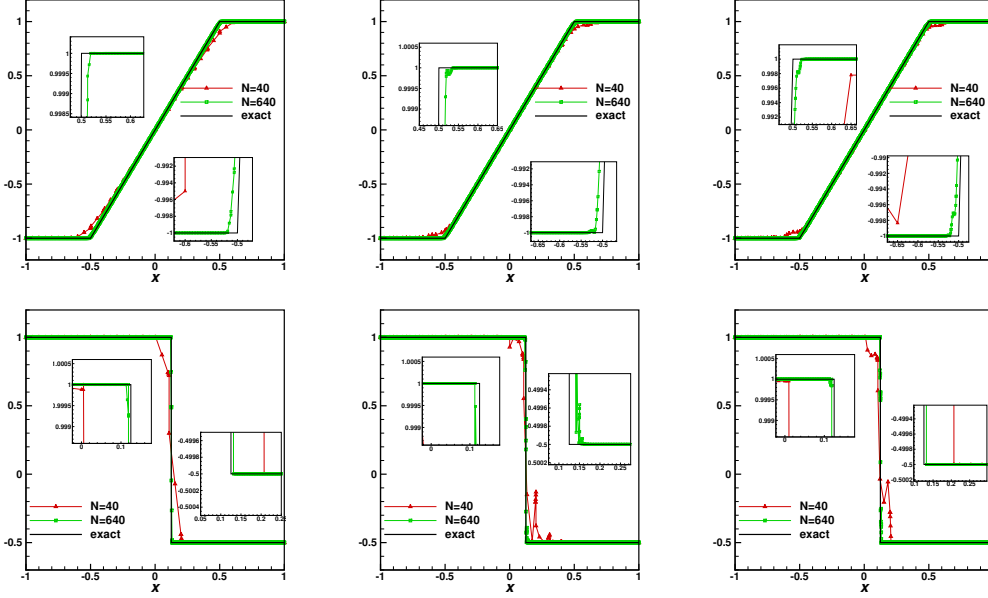


Figure 8: Numerical solutions of the Riemann problem for Burgers' equation at $t = 0.5$ based on polynomial degree p ($p = 1, 2, 3$ from left to right). Reconstruction on macro-elements and bound preserving limiter (3.23) are used in the computations. Top: a rarefaction wave. Bottom: a moving shock.

on the interface x_Γ . Thus, the conservation is satisfied. For how to guarantee conservation at the interface we refer to our previous work [18] (here we choose $\lambda_1 = 0, \lambda_2 = -1$). In Figure 9, the results from a third order scheme are shown at different time instances. In this case, the discontinuity is transported to the right until it reaches the interface. When the discontinuity enters the region where Burgers' equation holds, a rarefaction wave forms. With the proposed scheme, the solution is captured very well. Comparing the results ($h = 2/64$) in [1], our results are more accurate on the coarser mesh ($N=40, h = 1/20$) and the numerical solution is both conservative and satisfies the maximum principle. We also applied second order and fourth order schemes to solve this problem and the results are very similar.

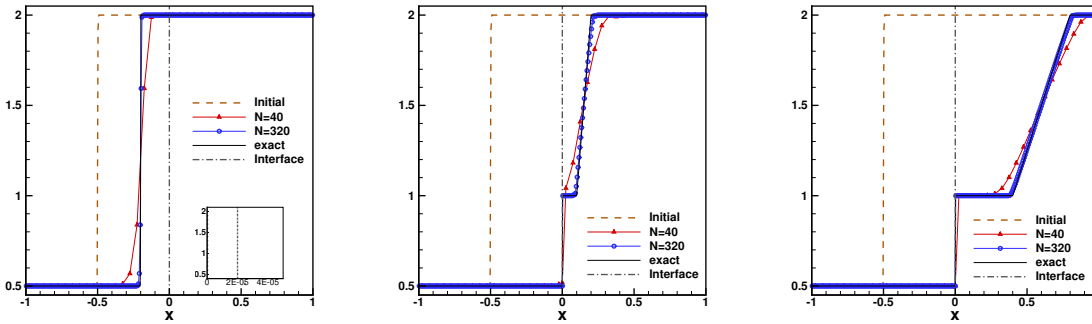


Figure 9: A third order approximation of a scalar hyperbolic conservation law with the discontinuous flux function (5.9) at different time instances. Left: $t = 0.3$, middle $t = 0.6$, right $t = 0.9$.

5.4 The Euler equations

In this subsection, we use our proposed Cut-DG method (3.1)-(3.3) with different piecewise polynomials, together with the positivity preserving limiter in Section 4.3 for Euler equations (4.1). Recall that each cut element is split into two parts of length α_k and $1 - \alpha_k$, with α_k defined in (5.1) and $\alpha = 0.01$. In the examples we consider $\gamma = 1.4$, which corresponds to an ideal gas.

5.4.1 Accuracy test: smooth problem

First, we consider a low density problem in one dimension. We take the initial condition as

$$\rho_0(x) = 1 + 0.99 \sin(x), \quad u_0 = 1, \quad p_0 = 1. \quad (5.11)$$

The domain is taken to be $[0, 2\pi]$. The exact solution of this problem is

$$\rho_0(x, t) = 1 + 0.99 \sin(x - t), \quad u(x, t) = 1, \quad p(x, t) = 1. \quad (5.12)$$

Without the positivity-preserving limiter the numerical scheme may be unstable due to the negative density in long time simulation. In Figure 10, we show the L^2 - and L^∞ -errors from our proposed bound-preserving Cut-DG methods at $t = 1$. We observe the optimal $p + 1$ -th order of accuracy for approximations of polynomial order $p = 1, 2, 3$.

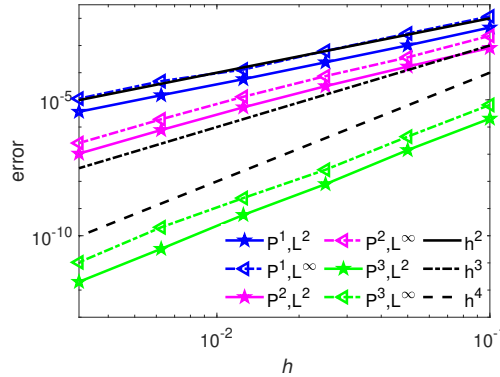


Figure 10: The L^2 - and L^∞ -errors for the numerical solutions of the low density problem in Section 5.3.1 from our proposed bound-preserving Cut-DG method.

5.4.2 Riemann problems

In this subsection, we consider two Riemann problems. We use the proposed bound preserving Cut-DG method (3.1)-(3.3) with spaces P^2, P^3 .

First, we consider the Sod shock tube problem in the domain $[0, 1]$. The initial condition is taken as

$$(\rho_L, u_L, p_L) = (1, 0, 1), \quad x < 0.5, \quad (\rho_R, u_R, p_R) = (0.125, 0, 0.1), \quad x > 0.5.$$

We solve this problem up to $t = 0.2$. The exact solution of Sod shock tube problem contains a rarefaction wave, a contact discontinuity and a shock discontinuity. Figure 11 shows the approximations of density (left), velocity (middle) and pressure (right) from our proposed bound-preserving Cut-DG scheme. In this

case, TVD limiting is needed to control oscillations. This limiter is applied to the reconstructed solutions on macro-elements before the positivity-preserving limiter is applied. We observe that our proposed Cut-DG scheme can simulate this Riemann problem well and can capture the rarefaction wave and discontinuities. Just as for the standard DG method [12] on a fitted mesh, when the TVD limiter is applied to the variables component-wise, we see some numerical artifacts in form of oscillations, which decrease with mesh refinement.

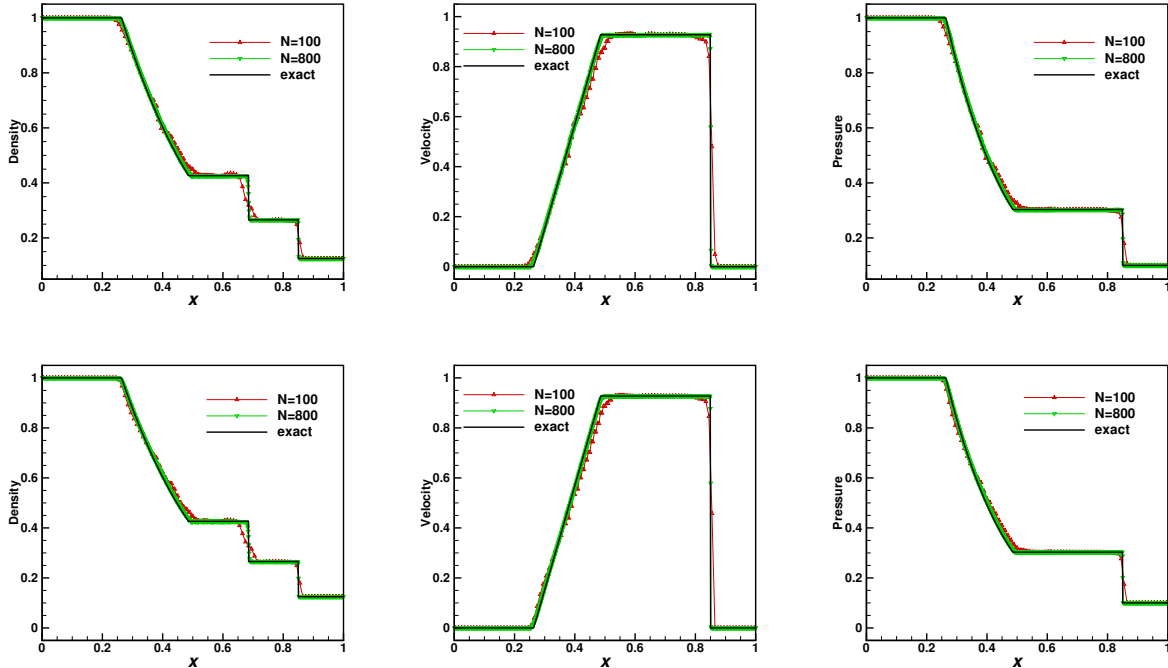


Figure 11: The numerical solutions from the proposed Cut-DG scheme for Sod shock tube problem on cut meshes. Top: P^2 approximations. Bottom: P^3 approximations.

The second Riemann problem is a double rarefaction wave in the domain $[-1, 1]$ as in [34]. The initial condition is

$$(\rho_L, u_L, p_L) = (7, -1, 0.2), \quad x < 0, \quad (\rho_R, u_R, p_R) = (7, 1, 0.2), \quad x > 0,$$

and outflow boundary conditions are used at both boundaries. There is no shock in this problem. Thus, only the positivity-preserving limiter is used for this problem. Notice that the exact solution contains almost a vacuum. In the middle and right panels of Figure 12 we show the results from our proposed Cut-DG method for Euler equations. The termination time is $t = 0.6$. In the left panel of Figure 12, we give the approximations of ρ, u, p from the standard DG method on uniform meshes with 800 elements. We observe that the results on cut meshes are practically similar to those on uniform meshes. For this Riemann problem computations are unstable without the positivity preserving limiter.

5.4.3 Sedov blast wave problem

We now test is the Sedov blast wave problem, a typical low-density problem with strong shocks. The exact solution can be found in [31, 43]. The computational domain is $[-2, 2]$, and we use $N = 200, 800$ elements

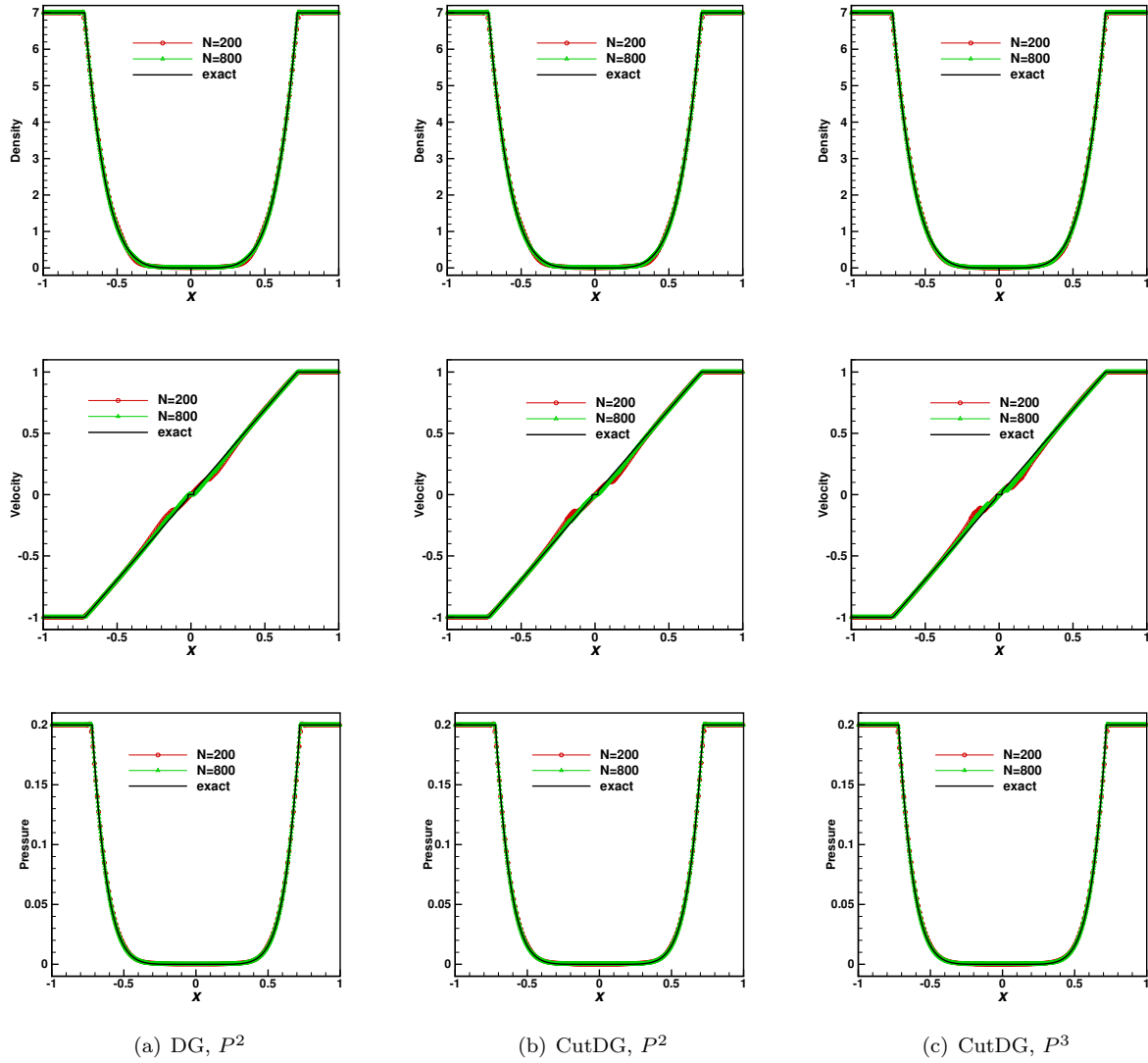


Figure 12: DG and CutDG approximations for the double rarefaction problem on the uniform mesh (left) and cut (middle, right) meshes. Solid line: exact solution. Symbol: approximations.

on the background mesh. We take the initial condition as

$$(\rho, u, E) = \begin{cases} (1, 0, 3.2 \cdot 10^6) & x \in [0, h] \\ (1, 0, 10^{-12}) & \text{otherwise,} \end{cases}$$

where $h = 4/N$. The elements in $[-0.5, 0.5]$ are cut with $\alpha = 0.01$. We simulate this problem up to time $t = 0.001$ with P^2 approximations by our proposed scheme. We apply a TVD limiter to the reconstructed approximation on the macro-elements and the positivity preserving limiter is applied to modify the limited approximation to make sure the solution has positive density and pressure. In the top panel of Figure 13, we observe that our proposed Cut-DG method (3.1)-(3.3) together with the positivity preserving limiter in Section 4.3 can simulate this blast wave problem very well. To minimize errors and reduce computational costs, we also simulated this problem using the scheme (3.1). The TVD limiter was applied to the unreconstructed solution on the macro-elements. Then, we reconstructed the solution on those macro-elements where the numerical solution had negative density or pressure, and a positivity-preserving limiter was applied to the reconstruction on the macro-elements. The results are shown in the bottom panel of Figure 13, which demonstrate that the locally applied reconstruction can also simulate this problem effectively.

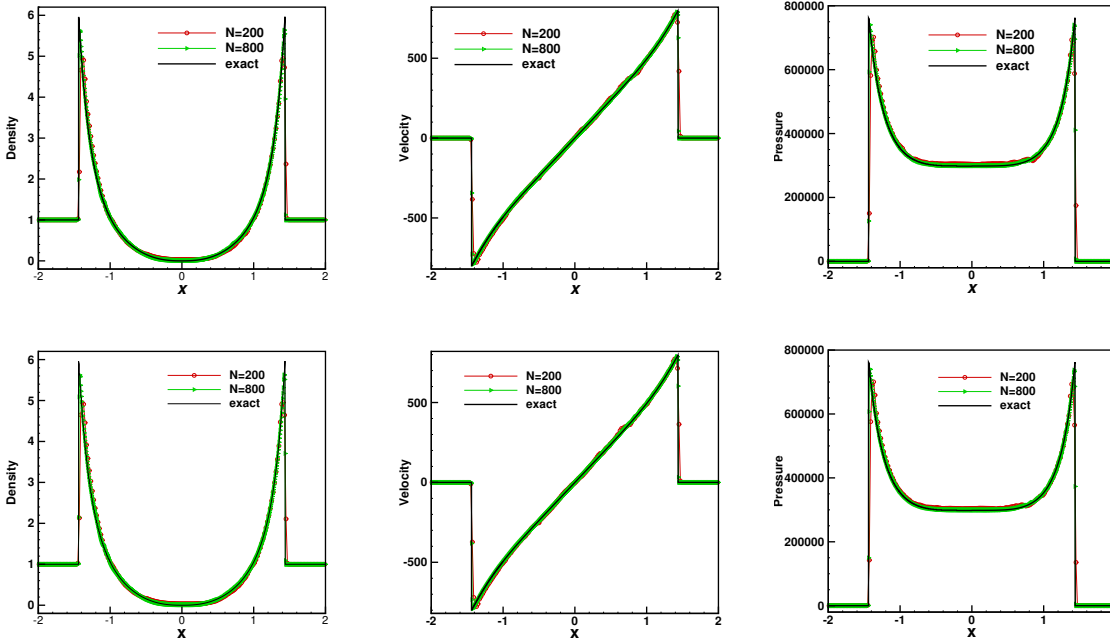


Figure 13: The third order Cut-DG approximation of Sedov blast wave on the cut mesh. The solid line is the exact solution and the symbols represents the Cut-DG solutions. Top: reconstruction on all macro-elements. Bottom: reconstruction only on macro-elements where the numerical solution has negative density or pressure.

5.4.4 The two blast wave problem

Finally, we consider the two blast wave problem for the Euler Equations with solid wall boundary conditions, see [50]. The solution contains strong shocks and rarefactions, which are reflected multiple times at the solid boundaries. There are a variety of interactions between shock waves and rarefaction waves, as well as between

these waves and contact discontinuities. We consider the problem on the physical domain $[x_l, x_r] = [0, 1]$, which is immersed in a background mesh. In this example there are only cut elements at the boundaries. We have constructed the mesh to be the same as in [48, 51], where the inverse Lax-Wendroff method is used. We take the computational domain as $[x_L, x_R]$ with $x_L = x_l - (1 - \alpha)h$, $x_R = x_r + (1 - \alpha)h$ and a uniform grid $x_L = x_{-\frac{1}{2}} < x_{\frac{1}{2}} < \dots < x_{N-\frac{1}{2}} < x_{N+\frac{1}{2}} = x_R$. As in [51], two unfitted small cells with size αh appear at the boundaries. In our computations $\alpha = 0.01$. The initial data at $t = 0$ is taken as

$$(\rho, u, p) = \begin{cases} (1, 0, 10^3) & 0 < x < 0.1, \\ (1, 0, 10^{-2}) & 0.1 < x < 0.9, \\ (1, 0, 10^2) & 0.9 < x < 1. \end{cases} \quad (5.13)$$

At the boundaries, we use wall boundary conditions. We solve this problem by our proposed positivity-preserving scheme up to $t = 0.038$. The numerical solution of density is shown in Figure 14. We use the solution from the third order standard DG method on uniform mesh with $h = 1/3200$ as the reference solution. We can see that our proposed scheme can capture the structure of the solution well and preserve the positivity of density and pressure.

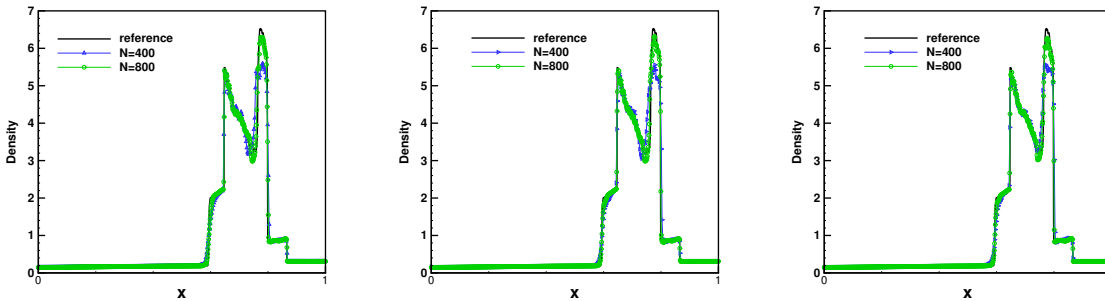


Figure 14: Example 5.3: numerical approximations of density at $t = 0.038$ for the two blast wave problem. Circle: numerical solution from our proposed scheme. Solid: reference solution from the standard DG method. P^1, P^2, P^3 approximation from left to right.

6 Conclusion

In this paper, we present a family of bound preserving Cut-DG methods for hyperbolic conservation laws. The methods are based on explicit time-stepping with time-step restrictions on the same order as for the corresponding standard DG methods on un-cut meshes. The parameter $0 < \delta \leq 1$ in (2.8) regulates when cut-elements are stabilized, and influences the time-step restriction. By choosing $\delta = 1$ we get exactly the same time-step restriction as in the standard un-cut case, but all cut elements are stabilized.

A new reconstruction of the solution on macro-elements is introduced as a post-processing step in each inner stage of each time step. It ensures that our proposed piecewise constant scheme satisfies the maximum principle for scalar conservation laws and positivity of density and pressure for the system of Euler equations, respectively. The higher order versions of our proposed method includes bound preserving limiting applied to the reconstruction on the macro-elements. To avoid oscillations when discontinuities are present, additional limiting is also included. Results from numerical computations demonstrate the good properties of our

proposed methodology. The test cases include several challenging problems for the Euler equations, such as the Sedov blast wave and a double rarefaction problem. These examples include regions of low density and strong shocks.

Extending the methodology to higher space dimensions is straightforward when no limiting is needed, and we have good preliminary results for smooth solutions. We also have good results when including bound preserving limiting for elements of polynomial orders zero and one. For polynomial orders higher than one, a good strategy for finding minimal/maximal values on irregular domains (which is needed in the bound preserving limiter) needs to be developed. We hope to present more complete results for problems in higher space dimensions in the future.

A Fully discrete algorithm for the Euler equations

In this appendix, the fully discrete algorithm for the Euler equations is shown in Algorithm 2.

Reference

- [1] J. Badwaik and A. M. Ruf. Convergence rates of monotone schemes for conservation laws with discontinuous flux. *SIAM Journal on Numerical Analysis*, 58(1):607–629, 2020.
- [2] P. Batten, N. Clarke, C. Lambert, and D. M. Causon. On the choice of wavespeeds for the HLLC Riemann solver. *SIAM Journal on Scientific Computing*, 18(6):1553–1570, 1997.
- [3] M. Berger and A. Giuliani. A state redistribution algorithm for finite volume schemes on cut cell meshes. *Journal of Computational Physics*, 428:109820, 2021.
- [4] E. Burman. Ghost penalty. *Comptes Rendus Mathematique*, 348(21-22):1217–1220, 2010.
- [5] E. Burman and P. Hansbo. Fictitious domain finite element methods using cut elements: II. A stabilized Nitsche method. *Applied Numerical Mathematics*, 62(4):328–341, 2012.
- [6] E. Burman, P. Hansbo, and M. G. Larson. CutFEM based on extended finite element spaces. *Numerische Mathematik*, 152(2):331–369, 2022.
- [7] E. Burman, P. Hansbo, and M. G. Larson. Explicit time stepping for the wave equation using *cut fem* with discrete extension. *SIAM Journal on Scientific Computing*, 44(3):A1254–A1289, 2022.
- [8] G. Chen, R. Pan, and S. Zhu. Singularity formation for the compressible Euler equations. *SIAM Journal on Mathematical Analysis*, 49(4):2591–2614, 2017.
- [9] Z. Chen, K. Li, and X. Xiang. An adaptive high-order unfitted finite element method for elliptic interface problems. *Numerische Mathematik*, 149(3):507–548, 2021.
- [10] Z. Chen and Y. Liu. An arbitrarily high order unfitted finite element method for elliptic interface problems with automatic mesh generation. *Journal of Computational Physics*, 491:112384, 2023.
- [11] B. Cockburn, S. Hou, and C.-W. Shu. The Runge-Kutta local projection discontinuous Galerkin finite element method for conservation laws. IV. The multidimensional case. *Mathematics of Computation*, 54(190):545–581, 1990.

- [12] B. Cockburn, S.-Y. Lin, and C.-W. Shu. TVB Runge-Kutta local projection discontinuous Galerkin finite element method for conservation laws III: One-dimensional systems. *Journal of Computational Physics*, 84(1):90 – 113, 1989.
- [13] B. Cockburn and C.-W. Shu. TVB Runge-Kutta local projection discontinuous Galerkin finite element method for conservation laws. II. General framework. *Mathematics of computation*, 52(186):411–435, 1989.
- [14] B. Cockburn and C.-W. Shu. The Runge–Kutta discontinuous Galerkin method for conservation laws V: multidimensional systems. *Journal of Computational Physics*, 141(2):199–224, 1998.
- [15] C. M. Dafermos and C. M. Dafermos. *Hyperbolic conservation laws in continuum physics*, volume 3. Springer, 2005.

Algorithm 2: Fully discrete bound preserving Cut-DG method for the Euler equations

Data: Given initial condition $\mathbf{u}_0(x)$ at $t = 0$

Result: Bound preserving approximation at final time T

```

1 Initialize  $\tilde{\mathbf{u}}_h^0$  by (2.14) and  $n = 0$ ;
2  $\mathbf{u}_h^0 =$  Reconstruction and limiting( $\tilde{\mathbf{u}}_h^0$ );
3 while  $t \leq T$  do
4   Compute suitable time-step  $\Delta t$  based on Theorem 4.1/4.2;
   /* Runge-Kutta time discretization                                     */
5    $\tilde{\mathbf{u}}_h^{(1)} =$  Euler-Step ( $\mathbf{u}_h^n, t_n, \Delta t$ );                               // first stage
6    $\mathbf{u}_h^{(1)} =$  Reconstruction and limiting ( $\tilde{\mathbf{u}}_h^{(1)}$ );
7    $\mathbf{u}_h^{(2')} =$  Euler-Step( $\mathbf{u}_h^{(1)}, t_n + \Delta t, \Delta t$ );                       // second stage
8   Set:  $\tilde{\mathbf{u}}_h^{(2)} = \frac{3}{4}\mathbf{u}_h^n + \frac{1}{4}\mathbf{u}_h^{(2')}$ ;
9    $\mathbf{u}_h^{(2)} =$  Reconstruction and limiting ( $\tilde{\mathbf{u}}_h^{(2)}$ );
10   $\tilde{\mathbf{u}}_h^{(3')} =$  Euler-Step( $\mathbf{u}_h^{(2)}, t_n + \Delta t/2, \Delta t$ );                       // third stage
11  Set:  $\tilde{\mathbf{u}}_h^{(3)} = \frac{1}{3}\mathbf{u}_h^n + \frac{2}{3}\mathbf{u}_h^{(3')}$ ;
12   $\mathbf{u}_h^{(3)} =$  Reconstruction and limiting ( $\tilde{\mathbf{u}}_h^{(3)}$ );
13  Set:  $\mathbf{u}_h^{n+1} = \mathbf{u}_h^{(3)}$ ;
14   $n \leftarrow n + 1$ ;
15   $t \leftarrow t + \Delta t$ ;
16 end
1 Function Euler-step( $\mathbf{u}_h, t, \Delta t$ )
2   Using (3.1) with  $\mathbf{u}_h, t, \Delta t$  component-wise to get  $\tilde{\mathbf{u}}_h = (\tilde{\mathbf{u}}_{h,1}, \tilde{\mathbf{u}}_{h,2}, \dots, \tilde{\mathbf{u}}_{h,N_\Omega}) \in V_h^p$ ;
3   return  $\tilde{\mathbf{u}}_h = (\tilde{\mathbf{u}}_{h,1}, \tilde{\mathbf{u}}_{h,2}, \dots, \tilde{\mathbf{u}}_{h,N_\Omega})$ ;
1 Function Reconstruction and limiting( $\tilde{\mathbf{u}}_h$ )
2   for  $i = 1$  to  $N_\Omega$  do
3     Using (3.2) with  $\tilde{\mathbf{u}}_h$  component-wise to reconstruct  $\mathbf{u}_{h,i}^M, i = 1, \dots, N_\Omega$ ;
4     if  $\mathbf{u}_{h,i}^M|_{\Omega_i} \notin G$  then modify  $\mathbf{u}_{h,i}^M$  by (4.14)-(4.18);
5      $u_{h,i} \leftarrow u_{h,i}^M$ ;
6   end
7   return  $\mathbf{u}_h = (u_{h,1}, \mathbf{u}_{h,2}, \dots, \mathbf{u}_{h,N_\Omega}) \in V_h^p$ ;

```

- [16] C. Engwer, S. May, A. Nüßing, and F. Streitbürger. A stabilized DG cut cell method for discretizing the linear transport equation. *SIAM Journal on Scientific Computing*, 42(6):A3677–A3703, 2020.
- [17] T. Frachon and S. Zahedi. A cut finite element method for incompressible two-phase Navier–Stokes flows. *Journal of Computational Physics*, 384:77–98, 2019.
- [18] P. Fu, T. Frachon, G. Kreiss, and S. Zahedi. High order discontinuous cut finite element methods for linear hyperbolic conservation laws with an interface. *Journal of Scientific Computing*, 90(3):1–39, 2022.
- [19] P. Fu and G. Kreiss. High order cut discontinuous Galerkin methods for hyperbolic conservation laws in one space dimension. *SIAM Journal on Scientific Computing*, 43(4):A2404–A2424, 2021.
- [20] P. Fu and Y. Xia. The positivity preserving property on the high order arbitrary Lagrangian–Eulerian discontinuous Galerkin method for Euler equations. *Journal of Computational Physics*, 470:111600, 2022.
- [21] A. Giuliani. A two-dimensional stabilized discontinuous Galerkin method on curvilinear embedded boundary grids. *SIAM Journal on Scientific Computing*, 44(1):A389–A415, 2022.
- [22] J. Glimm. Solutions in the large for nonlinear hyperbolic systems of equations. *Communications on Pure and Applied Mathematics*, 18:697–715, 1965.
- [23] S. Gottlieb, C.-W. Shu, and E. Tadmor. Strong stability-preserving high-order time discretization methods. *SIAM review*, 43(1):89–112, 2001.
- [24] C. Gürkan, S. Stisko, and A. Massing. Stabilized cut discontinuous Galerkin methods for advection–reaction problems. *SIAM Journal on Scientific Computing*, 42(5):A2620–A2654, 2020.
- [25] Y. Ha, C. L. Gardner, A. Gelb, and C.-W. Shu. Numerical simulation of high Mach number astrophysical jets with radiative cooling. *Journal of Scientific Computing*, 24(1):29–44, 2005.
- [26] P. Hansbo, M. G. Larson, and S. Zahedi. A cut finite element method for a Stokes interface problem. *Applied Numerical Mathematics*, 85:90–114, 2014.
- [27] J. S. Hesthaven. *Numerical Methods for Conservation Laws*. Society for Industrial and Applied Mathematics, Philadelphia, PA, 2018.
- [28] J. S. Hesthaven and T. Warburton. *Nodal discontinuous Galerkin methods: algorithms, analysis, and applications*. Springer Science & Business Media, 2007.
- [29] P. Huang, H. Wu, and Y. Xiao. An unfitted interface penalty finite element method for elliptic interface problems. *Computer Methods in Applied Mechanics and Engineering*, 323:439–460, 2017.
- [30] A. Johansson and M. G. Larson. A high order discontinuous Galerkin Nitsche method for elliptic problems with fictitious boundary. *Numerische Mathematik*, 123(4):607–628, Apr 2013.
- [31] V. P. Korobeinikov. *Problems of point blast theory*. Springer Science & Business Media, 1991.
- [32] F. Kummer. Extended discontinuous Galerkin methods for two-phase flows: the spatial discretization. *International Journal for Numerical Methods in Engineering*, 109(2):259–289, 2017.
- [33] M. G. Larson and S. Zahedi. Conservative cut finite element methods using macroelements. *Computer Methods in Applied Mechanics and Engineering*, 414:116141, 2023.

- [34] T. Linde, P. Roe, T. Linde, and P. Roe. Robust Euler codes. In *13th computational fluid dynamics conference*, page 2098, 1997.
- [35] A. Massing, M. G. Larson, A. Logg, and M. E. Rognes. A stabilized Nitsche fictitious domain method for the Stokes problem. *Journal of Scientific Computing*, 61(3):604–628, 2014.
- [36] R. Massjung. An unfitted discontinuous Galerkin method applied to elliptic interface problems. *SIAM Journal on Numerical Analysis*, 50(6):3134–3162, 2012.
- [37] S. May and F. Streitbürger. DoD Stabilization for non-linear hyperbolic conservation laws on cut cell meshes in one dimension. *Applied Mathematics and Computation*, 419:126854, 2022.
- [38] J. Modisette and D. Darmofal. Toward a robust, higher-order cut-cell method for viscous flows. In *48th AIAA Aerospace Sciences Meeting Including the New Horizons Forum and Aerospace Exposition*, page 721, 2010.
- [39] B. Müller, S. Krämer-Eis, F. Kummer, and M. Oberlack. A high-order discontinuous Galerkin method for compressible flows with immersed boundaries. *International Journal for Numerical Methods in Engineering*, 110(1):3–30, 2017.
- [40] R. Qin and L. Krivodonova. A discontinuous Galerkin method for solutions of the Euler equations on Cartesian grids with embedded geometries. *Journal of Computational Science*, 4(1-2):24–35, 2013.
- [41] J. Qiu and C.-W. Shu. Runge–Kutta Discontinuous Galerkin Method Using WENO Limiters. *SIAM Journal on Scientific Computing*, 26(3):907–929, 2005.
- [42] S. Schoeder, S. Sticker, G. Kreiss, and M. Kronbichler. High-order cut discontinuous Galerkin methods with local time stepping for acoustics. *International Journal for Numerical Methods in Engineering*, 121(13):2979–3003, 2020.
- [43] L. I. Sedov. *Similarity and dimensional methods in mechanics*. CRC press, 1993.
- [44] C.-W. Shu. Discontinuous Galerkin methods: general approach and stability. *Numerical solutions of partial differential equations*, pages 149–201, 2009.
- [45] E. M. Stein. *Singular Integrals and Differentiability Properties of Functions (PMS-30), Volume 30*. Princeton university press, 2016.
- [46] S. Sticker and G. Kreiss. A stabilized Nitsche cut element method for the wave equation. *Computer Methods in Applied Mechanics and Engineering*, 309:364–387, 2016.
- [47] S. Sticker and G. Kreiss. Higher order cut finite elements for the wave equation. *Journal of Scientific Computing*, 80(3):1867–1887, 2019.
- [48] S. Tan and C.-W. Shu. Inverse lax-wendroff procedure for numerical boundary conditions of conservation laws. *Journal of Computational Physics*, 229(21):8144–8166, 2010.
- [49] E. Toro. *Riemann Solvers and Numerical Methods for Fluid Dynamics: A Practical Introduction*. 01 2009.
- [50] P. Woodward and P. Colella. The numerical simulation of two-dimensional fluid flow with strong shocks. *Journal of computational physics*, 54(1):115–173, 1984.

- [51] L. Yang, S. Li, Y. Jiang, C.-W. Shu, M. Zhang, and Z.-C. Shi. Inverse lax-wendroff boundary treatment of discontinuous galerkin method for 1d conservation laws.
- [52] X. Zhang and C.-W. Shu. On maximum-principle-satisfying high order schemes for scalar conservation laws. *Journal of Computational Physics*, 229(9):3091–3120, 2010.
- [53] X. Zhang and C.-W. Shu. On positivity-preserving high order discontinuous Galerkin schemes for compressible Euler equations on rectangular meshes. *Journal of Computational Physics*, 229(23):8918–8934, 2010.